Christine M. Kusminski,[1] Shiuhwei Chen,[2,3] Risheng Ye,[1] Kai Sun,[1] Qiong A. Wang,[1] Stephen B. Spurgin,[1] Phillip E. Sanders,[4] Joseph T. Brozinick,[4] Werner J. Geldenhuys,[5] Wen-hong Li,[2,3] Roger H. Unger,[1] and Philipp E. Scherer[1,2]

MitoNEET-Parkin Effects in Pancreatic α- and β-Cells, Cellular Survival, and Intrainsular Cross Talk

Diabetes 2016;65:1534–1555 | DOI: 10.2337/db15-1323

Mitochondrial metabolism plays an integral role in glucose-stimulated insulin secretion (GSIS) in β-cells. In addition, the diabetogenic role of glucagon released from α-cells plays a major role in the etiology of both type 1 and type 2 diabetes because unopposed hyperglucagonemia is a pertinent contributor to diabetic hyperglycemia. Titrating expression levels of the mitochondrial protein mitoNEET is a powerful approach to fine-tune mitochondrial capacity of cells. Mechanistically, β-cell–specific mitoNEET induction causes hyperglycemia and glucose intolerance due to activation of a Parkin-dependent mitophagic pathway, leading to the formation of vacuoles and uniquely structured mitophagosomes. Induction of mitoNEET in α-cells leads to fasting-induced hypoglycemia and hypersecretion of insulin during GSIS. MitoNEET-challenged α-cells exert potent antiapoptotic effects on β-cells and prevent cellular dysfunction associated with mitoNEET overexpression in β-cells. These observations identify that reduced mitochondrial function in α-cells exerts potently protective effects on β-cells, preserving β-cell viability and mass.

The critical roles mitochondria play in numerous aspects of metabolic regulation position them center stage in the regulation of energy homeostasis. Pancreatic β-cells are glucose sensors that adjust insulin release to blood glucose levels to sustain euglycemia, a process where mitochondria are integral to coupling glucose metabolism with insulin exocytosis (1). The pertinent role of ATP production in β-cells is reflected by the blockade of glucose-stimulated insulin secretion (GSIS) with inhibition of mitochondrial electron transport chain complexes (2,3).

Obesity-associated type 2 diabetes mellitus (T2DM) is characterized by insulin resistance such that β-cells are unable to appropriately compensate with elevated insulin secretion (4). Reduced β-cell volume, caused by β-cell death from glucolipotoxicity, results in low GSIS by residual β-cells in patients with diabetes (5,6). Mitochondrial dysfunction in β-cells plays a pivotal role in the anomalies of obesity-related T2DM (7,8). Impaired β-cell function is associated with mitochondrial DNA mutations in humans and is induced in rodents by using β-cell–specific deletions of targeted mitochondrial genes; in both cases, low oxidative capacity and β-cell dysfunction ensue (6,9). Mitochondria in β-cells in patients with diabetes also exhibit morphologic and functional abnormalities, concurrent with compromised function (5,6). The precise mechanisms that impede mitochondrial function and the key pathways that activate β-cell failure and loss of β-cell mass remain unknown (4). Delineating mechanisms that perturb mitochondrial β-cell function should help to define the pathophysiology of β-cell dysfunction in T2DM and identify novel avenues that preserve β-cell mass.

MitoNEET has been identified as a dimeric mitochondrial membrane protein (10,11). Located on the outer mitochondrial membrane (OMM), mitoNEET was named according to its COOH-terminal amino acid sequence Asn-Glu-Glu-Thr (NEET) (10). Oriented toward the cytoplasm, mitoNEET binds redox-active 2Fe-2S clusters (12–14). We previously determined that in white adipose tissue (WAT),

[1]Touchstone Diabetes Center, Department of Internal Medicine, The University of Texas Southwestern Medical Center, Dallas, TX
[2]Department of Cell Biology, The University of Texas Southwestern Medical Center, Dallas, TX
[3]Department of Biochemistry, The University of Texas Southwestern Medical Center, Dallas, TX
[4]Lilly Research Laboratories, Division of Eli Lilly and Co., Indianapolis, IN
[5]Department of Pharmaceutical Sciences, School of Pharmacy, West Virginia University, Morgantown, WV

Corresponding author: Philipp E. Scherer, philipp.scherer@utsouthwestern.edu.

Received 21 September 2015 and accepted 6 February 2016.

This article contains Supplementary Data online at http://diabetes.diabetesjournals.org/lookup/suppl/doi:10.2337/db15-1323/-/DC1.

See accompanying article, p. 1484.

mitoNEET lowers mitochondrial oxidative capacity; this triggers a profound compensatory response in the mature adipocyte such that peroxisome proliferator–activated receptor-γ (PPARγ) and adiponectin levels increase to activate massive WAT expansion (15). MitoNEET achieves these remarkable metabolic effects by acting as a powerful regulator of iron content in the mitochondrial matrix (15).

Glucagon secretion from α-cells sustains glucose levels during fasting by stimulating hepatic glucose production (16). When glucose demand is increased, insulin secretion falls, thus stimulating glucagon production and removing the inhibitory action of insulin on the liver while augmenting the stimulatory effect of glucagon on gluconeogenesis (17). Conversely, under nutrient excess, the reverse occurs. The hepatic effects of insulin and glucagon are in diametric opposition, with both regulating glucose metabolism to preserve normoglycemia. This finely tuned balance is perturbed in patients with diabetes (18). Fasting and postprandial hyperglucagonemia exist alongside insulin insufficiency and enhanced hepatic glucose output, both contributors to hyperglycemia (19,20). Preclinical studies also demonstrate that postabsorptive hyperglucagonemia accounts for ~50% of the pathological increment in glucose excursions (21). Therefore, targeting α-cell–derived glucagon excess to eliminate diabetic glycemic volatility is appealing for the treatment of T2DM such that novel avenues aimed to suppress glucagon hypersecretion or signaling should prove beneficial (20). Although how mitochondria affect glucagon secretion from α-cells is unknown, identifying strategies that target α-cell mitochondrial function, with the aim of curbing glucagon secretion during T2DM, is a widely unexplored area. Preserving insulin secretion and preventing loss of β-cell mass while suppressing local glucagon production during insulin resistance are attractive therapeutic avenues. We used mitoNEET as a unique modulator of mitochondrial activity to influence whole-islet physiology by inducing the protein either in β-cells, α-cells, or both cell types simultaneously. The hope was to unravel the critical mechanisms by which compromised mitochondrial function alters β-cell insulin secretion and α-cell glucagon production with the goal of preserving insulin sensitivity under metabolic challenge.

RESEARCH DESIGN AND METHODS

Animals

All animal experimental protocols were approved by the Institutional Animal Care and Use Committee of The University of Texas Southwestern (UTSW) Medical Center (Dallas, TX). Tet-responsive element (*TRE*)-*mitoNEET* mice were generated as previously described (15). Mouse insulin promoter (*MIP*)-*rtTA* mice and preproglucagon (*PPG*)-*rtTA* mice were generated by subcloning the rtTA into a plasmid containing the 8.3-kilobase (kb) MIP or the 1.7-kb PPG promoter, respectively. After linearization, the construct was injected into C57/BL6-derived blastocysts. *TRE-LacZ* and Parkin knockout (*Park-KO*) mice were purchased from The Jackson Laboratory (Bar Harbor, ME). Transgene-positive offspring were genotyped with PCR by using the following primer sets: *TRE-mitoNEET*, 5′-AGAGAATCGCAC CAAAGCTATG and 5′-CAAACTCACCCTGAAGTTCTCAG; TRE-LacZ, 5′-ATCCTCTGCATGGTCAGGTC and 5′-CGTGG CCTGATTCATTCC; TRE-green fluorescent protein (GFP), 5′- GTAAACGGCCACAAGTTCAGC and 5′-GATGCCGTTCTTC TGCTTGTC; *MIP-rtTA*, 5′-CACCTGGAGACCTTAATGGGC CAAAC and 5′-CGATTGGCAGGGCATCGAGC; *PPG-rtTA*, 5′-TTTGAACAGAAGGGGCTTTTT and 5′-GAGCGAGTTTCCT TGTCGTC; *Park-KO* mutant, 5′-ATGTTGCCGTCCTCCTTGA AGTCG and Parkin wild-type (WT), 5′-GCAGAATTACAG CAGTTACCTGG and 5′-CCTACACAGAACTGTGACCTGG (all three primers mixed in one reaction). All experiments were performed in a pure C57/BL6 background and conducted using male and female littermate control mice. All doxycycline (Dox)-chow diet (25, 50, 100, or 600 mg/kg Dox) or Dox high-fat diet (HFD) (600 mg/kg Dox) experiments were initiated at ~6–12 weeks of age. Mice were fed a pioglitazone (Pio)-containing (40 mg/kg/day; Watson Pharmaceuticals) Dox chow (600 mg/kg) diet.

Systemic Tests

For the oral glucose tolerance test (OGTT), mice were fasted for 3 h before administration of glucose 2.5 g/kg body weight (BW) by gastric gavage. For the arginine tolerance test, mice were fasted overnight (12–16 h) before intraperitoneal injection of L-arginine 1 mg/g BW (Sigma-Aldrich). At the indicated time points, venous blood samples from the tail vein were collected in heparin-coated capillary tubes. Glucose levels were determined by using an oxidase-peroxidase assay (Sigma-Aldrich, St. Louis, MO). Insulin levels were measured with commercially available ELISA kits (Millipore LINCO Research, St. Charles, MO). Pancreatic insulin content was measured as previously described (22). Glucagon levels were measured by using an ELISA kit (Mercodia Inc., Winston-Salem, NC).

GSIS on Perfused Pancreata

Mouse pancreata were perfused with buffers containing either 2.7 mmol/L or 16.7 mmol/L glucose (Sigma-Aldrich). All buffers before reaching the celiac artery were maintained at 37°C. Perfusates were then collected at 1-min intervals for 25 min. Insulin levels were measured in perfusates with an insulin assay kit (Cisbio).

Isolation of Islets

Mice were sacrificed by cervical dislocation after isoflurane anesthesia, then pancreatic islets were isolated as previously detailed (23). Briefly, pancreata were inflated using Liberase TL 0.1 g/L (#05401020001; Roche) containing DNase I 0.1 g/L (#10104159001; Roche) and then digested by incubation at 37°C for 25 min. Islets were hand selected under a dissection microscope, washed in sterile 1× PBS, and immediately snap frozen in liquid nitrogen followed by storage at −80°C until analysis.

Isolation of GFP-Labeled α-Cells by FACS Sorting

After islet isolation, every 70–80 islets (mixed sizes) were handpicked and added to a tube containing 500 μL enzyme-free cell dissociation solution (Cat. S-004-B; Millipore). Islets

were allowed to dissociate in a 37°C water bath for 5–7 min before gently pipetting up and down until no visual clumps were observed. This procedure was repeated once. A small aliquot of islet suspension was examined under a light microscope to confirm the presence of a dispersed cell suspension. Cells were immediately centrifuged (4°C at 500*g* for 5 min) to remove the supernatant and then resuspended in 500 μL cold sample application buffer (114 mmol/L NaCl, 4.7 mmol/L KCl, 1.2 mmol/L KH_2PO4, 1.16 mmol/L $MgSO_4$, 20 mmol/L HEPES, and 2.5 mmol/L $CaCl_2$; pH 7.3) containing 5 mmol/L glucose and 1% FBS. This procedure was repeated once. All dispersed cells from the same group were pooled together and washed again. The final cell pellets were diluted to 0.5–1 × 10^6 cells/mL for FACS sorting. Cells were sorted by a BD FACSAria with an argon laser beam tuned to 488 nm at 50-mW output with a 530 ± 10 nm emission filter. C57/BL6 cells were used as the control and to set the sorting parameters. Cells were sorted at a rate of 1,000 events/s by using normal recovery mode with the temperature setting at 4°C.

Quantitative Real-Time PCR

Pancreatic tissues were excised from mice and snap frozen in liquid nitrogen. Total RNA was isolated after tissue homogenization in TRIzol (Invitrogen, Carlsbad, CA) using a TissueLyser (MagNA Lyser; Roche) and then isolated using an RNeasy RNA extraction kit (QIAGEN). The quality and quantity of RNA was determined by absorbance at 260/280 nm. cDNA was prepared by reverse transcribing 1 μg of RNA with an iScript cDNA Synthesis Kit (Bio-Rad, Hercules CA). Supplementary Table 2 details the primer sequences used for quantitative real-time PCR. Results were calculated by threshold cycle method (24), with β-actin used for normalization.

Histology, Immunofluorescence, and Immunohistochemistry

Pancreata were dissected and fixed in 10% PBS-formalin for 24 h. After paraffin embedding and sectioning (5 μm), tissues were stained with hematoxylin-eosin (H-E). For immunofluorescence (IF) and immunohistochemistry (IHC), paraffin-embedded sections were incubated with primary antibodies for 24 h at 4°C and subsequently decorated with secondary antibodies for 1 h at room temperature (RT). Antibodies used were a polyclonal anti-mitoNEET antibody (1:250; Santa Cruz Biotechnology, Dallas, TX), a guinea pig anti-swine insulin antibody (1:500; Dako, Carpinteria, CA), a rabbit antiglucagon antibody (1:250; Zymed, Grand Island, NY), and a polyclonal goat beclin-1 antibody (1:250; Santa Cruz Biotechnology). For IHC, sections were incubated with biotinylated secondary antibodies (anti-guinea pig antibody [1:500], anti-rabbit antibody [1:200], or anti-goat antibody [1:500]; Dako) for 1 h at RT, then reactions were developed using DAB (3,3'-diaminobenzidine) chromogen and DAB substrate buffer (Dako). All images were acquired with an Olympus FSZ100 light microscope or a Zeiss AxioObserver epifluorescence microscope. For microtubule-associated protein light chain 3 (LC3-II) IF staining, isolated islets were treated for 30 min at 37°C with a mixture containing CYTO-ID Green Detection Reagent Hoechst 33342 Nuclear Stain per manufacturer protocol (CYTO-ID Autophagy Detection Kit; Enzo Life Sciences, Inc., Farmingdale, NY). As a positive control, WT islets were pretreated with rapamycin (500 nmol/L). Islets were then washed twice with 1× assay buffer and transferred to a glass microscope slide. Autophagic signal was imaged by using confocal microscopy in the fluorescein isothiocyanate 488-nm excitable green fluorescent detection range (Leica TCS SP5 confocal microscope).

β-Galactosidase Staining of Tissues

Mice at age 10–12 weeks were anesthetized and perfused with 0.2% glutaraldehyde in 1× PBS. Pancreatic, gastric fundal, small intestinal, eye, and brain tissues were excised and placed into a 6-cm cell culture dish containing 0.2% glutaraldehyde and cut into small slices. Tissues were washed with rinse buffer (100 mmol/L sodium phosphate, 2 mmol/L $MgCl_2$, 0.01% sodium deoxycholate, and 0.02% NP-40) three times and then soaked in β-galactosidase (β-gal) staining buffer (5 mmol/L potassium ferricyanide, 5 mmol/L potassium ferrocyanide, and 1 mg/mL β-gal substrate in rinse buffer) for 48 h at RT with mild shaking. Tissues were transferred to 10% formalin overnight for postfixation, and postfixed tissues were processed with a standard paraffin tissue–embedding protocol. After paraffin embedding and sectioning, tissues were counterstained with nuclear fast red. Stained sections were imaged with an Olympus FSX100 light microscope.

Transmission Electron Microscopy

Fresh pancreatic tissues were fixed by perfusion with 4% paraformaldehyde and 1% glutaraldehyde in 0.1 mol/L sodium cacodylate buffer. Fixed tissues were transferred to 2.5% glutaraldehyde in 0.1 mol/L sodium cacodylate buffer, postfixed in buffered 1% osmium tetroxide, en bloc stained in 4% uranyl acetate in 50% ethanol, dehydrated with a graded series of ethanol, then embedded in EMbed 812 resin. Thin sections were cut on a Leica Ultracut UCT ultramicrotome and poststained with 2% uranyl acetate and lead citrate. Images were acquired on an FEI Tecnai G2 transmission electron microscope equipped with a LaB6 source and operating at 120 kV.

Immunoblotting

Frozen islets were homogenized in TNET buffer (50 mmol/L Tris-HCl [pH 7.6], 150 mmol/L NaCl, 5 mmol/L EDTA, phosphatase inhibitors [Sigma-Aldrich], protease inhibitors [Roche], and 1% Triton X-100) and then centrifuged at 13,000 rpm for 5 min. Protein concentrations were determined by using a bicinchoninic acid assay kit (Pierce). Proteins were resolved on 10–20% Tricine gels (Invitrogen) and then transferred to nitrocellulose membranes (Protran; Whatman GmbH, Dassel, Germany). Affinity-purified polyclonal anti-mitoNEET antibodies (1:1,000), monoclonal anti-Parkin antibodies (1:1,000; Cell Signaling Technology, Boston, MA), or monoclonal anti-β-actin antibodies (1:1,000) were used. Primary antibodies were detected with secondary IgG labeled with infrared dyes emitting at 700

and 800 nm (LI-COR Biosciences, Lincoln, NE) and then visualized on a LI-COR Odyssey infrared scanner. The scanned data were analyzed using Odyssey version 2.1 software (LI-COR Biosciences).

Mass Spectroscopy for Lipid Species Quantification

Lipid species were quantified, as previously detailed, by liquid chromatography and tandem mass spectrometry using a TSQ Quantum Ultra Triple Quadrupole Mass Spectrometer (Thermo Fisher Scientific) equipped with an electrospray ionization probe and interfaced with an Agilent 1100 series high-performance liquid chromatography system (Agilent Technologies) (25).

INS-1 Cell Culture and Plasmid Transfection

INS-1 cells were seeded on a 35-mm dish for 16–18 h before plasmid transfection at ~25% confluence. For each dish, 2.5 μg plasmid DNA (a cytomegalovirus [CMV]-mitoNEET-internal ribosome entry site [IRES]-GFP plasmid or a control CMV-GFP plasmid) was transfected into cells by using Lipofectamine 3000 (L3000-008; Invitrogen). After transfection (20–24 h), cells were imaged using a Zeiss LSM 780 confocal microscope. The GFP imaging was set at excitation 488 nm and emission 500–530-nm band path. The tetramethylrhodamine, methyl ester (TMRM) imaging was set at excitation 543 nm and emission 565–615-nm band path.

TMRM Staining and Carbonyl Cyanide-4-Phenylhydrazone Treatment

After plasmid transfection (20–24 h), INS-1 cells were washed three times with 1× PBS and then incubated with TMRM 20 nmol/L for 30 min at RT. The cells were washed three times with 1× PBS before imaging. As a control, carbonyl cyanide-4-phenylhydrazone 1 μmol/L was used to depolarize the mitochondria membrane potential ($\Delta\Psi_m$).

RESULTS

Generation of an Inducible β-Cell or α-Cell Labeling System

To create a system that allows us to induce any given protein specifically in β-cells, we generated a novel insulin promoter–driven reverse tetracycline-on controlled transactivator (*MIP-rtTA*) mouse. We also generated a novel PPG promoter–driven *rtTA* mouse (*PPG-rtTA*) that allows induction specifically in α-cells. MIP-rtTA and PPG-rtTA mRNA levels are highest and primarily restricted to the pancreas (Fig. 1*A* and 1*B*). To define the specificity, we used an inducible β-cell or α-cell labeling system. We crossed *MIP-rtTA* or *PPG-rtTA* mice with Tet-responsive LacZ (*TRE-LacZ*) mice. Upon Dox-chow feeding, β-cells or α-cells expressing rtTA activate the *TRE* promoter, and LacZ expression is induced only within these cell types. Tissues are then stained blue with β-gal substrate. Upon Dox-chow feeding, β-cells or α-cells of *TRE-LacZ-MIP-rtTA* or *TRE-LacZ-PPG-rtTA* mice were uniformly labeled blue (Fig. 1*C* and 1*D*), reflecting the presence of β-gal. Of note, β-cells within *TRE-LacZ-PPG-rtTA* islets were not labeled (Fig. 1*D*).

The rat insulin promoter cassette conveys expression in the hypothalamus (26). To confirm specificity of our inducible MIP–driven system, we stained brain slices from Dox-chow–fed *TRE-LacZ-MIP-rtTA* mice and observed no positive β-gal signal in the hypothalamus, cerebellum, or cerebrum (Supplementary Fig. 1*A*). Although we observed low *PPG-rtTA* gene expression in the whole brain (Fig. 1*B*), staining of hypothalamic, cerebellar, and cerebral tissues from *TRE-LacZ-PPG-rtTA* mice revealed no positive β-gal signal (Supplementary Fig. 1*B*), highlighting stringent pancreatic specificity of our *PPG-rtTA* mice. The *PPG* gene is also expressed in the intestinal endocrinocytes (L cells), albeit the tissue distribution diversifies during posttranslational processing (27). No positive β-gal signal was observed in small intestinal or colonic tissues from Dox-chow–fed *TRE-LacZ-PPG-rtTA* mice (Fig. 1*E*). The gastric fundus also is a source of glucagon in insulin-deprived depancreatized alloxan-diabetic dogs (28), suggesting that extrapancreatic glucagon contributes to hyperglucagonemia upon pancreatic injury. In animals with noncompromised pancreata, the current analyses revealed no β-gal signal in the gastric fundus (Supplementary Fig. 1*C*).

Induction of MitoNEET in β-Cells Causes Hyperglycemia, Glucose Intolerance, Cellular Dysfunction, and Loss of β-Cell Mass: A Novel and Highly Specific β-Cell Mouse Model of Titratable Diabetes

MitoNEET exerts a profound effect on whole-body energy utilization by lowering adipocyte mitochondrial iron content, which hinders mitochondrial function (15). The adipocyte compensates by upregulating PPARγ and adiponectin, which results in massive WAT expansion (15). We subsequently sought to explore whether mitoNEET influences pancreatic function and whether the β-cell activates compensatory mechanisms under mitochondrial dysfunction. We used the *TRE-mitoNEET* (*TRE-MitoN*) mouse (15) in which the expression of mitoNEET is driven by a tetracycline-inducible promoter element (or TRE). For the promoter element to be operational, the presence of the tetracycline-on transcription factor rtTA is necessary. We provide the rtTA factor in a β-cell– or α-cell–specific manner through mice harboring rtTA under the control of the MIP (Supplementary Fig. 2*A*) or the PPG promoter (Supplementary Fig. 2*B*), respectively. After Dox feeding, we achieved β-cell– or α-cell–specific induction of the mitoNEET transgene when *TRE-MitoN* mice were crossed with either *MIP-rtTA* mice or *PPG-rtTA* mice, respectively (Supplementary Fig. 2A and 2B). MitoNEET overexpression was strictly confined to the pancreas in *TRE-MitoN-MIP-rtTA* (*MIP-MitoN*) mice and *TRE-MitoN-PPG-rtTA* (*PPG-MitoN*) mice (Supplementary Fig. 2*C*) because endogenous mitoNEET levels in WT mice did not follow a comparable expression pattern (Supplementary Fig. 2*D*). IF staining revealed mitoNEET induction specifically in centrally located β-cells in *MIP-MitoN* islets (Supplementary Fig. 2*E*). In some β-cells, we saw a single prominent structure stained, whereas in other β-cells, we observed a more diffuse staining pattern. MitoNEET overexpression was also evident in peripherally located α-cells in *PPG-MitoN* islets (Supplementary Fig. 2*F*).

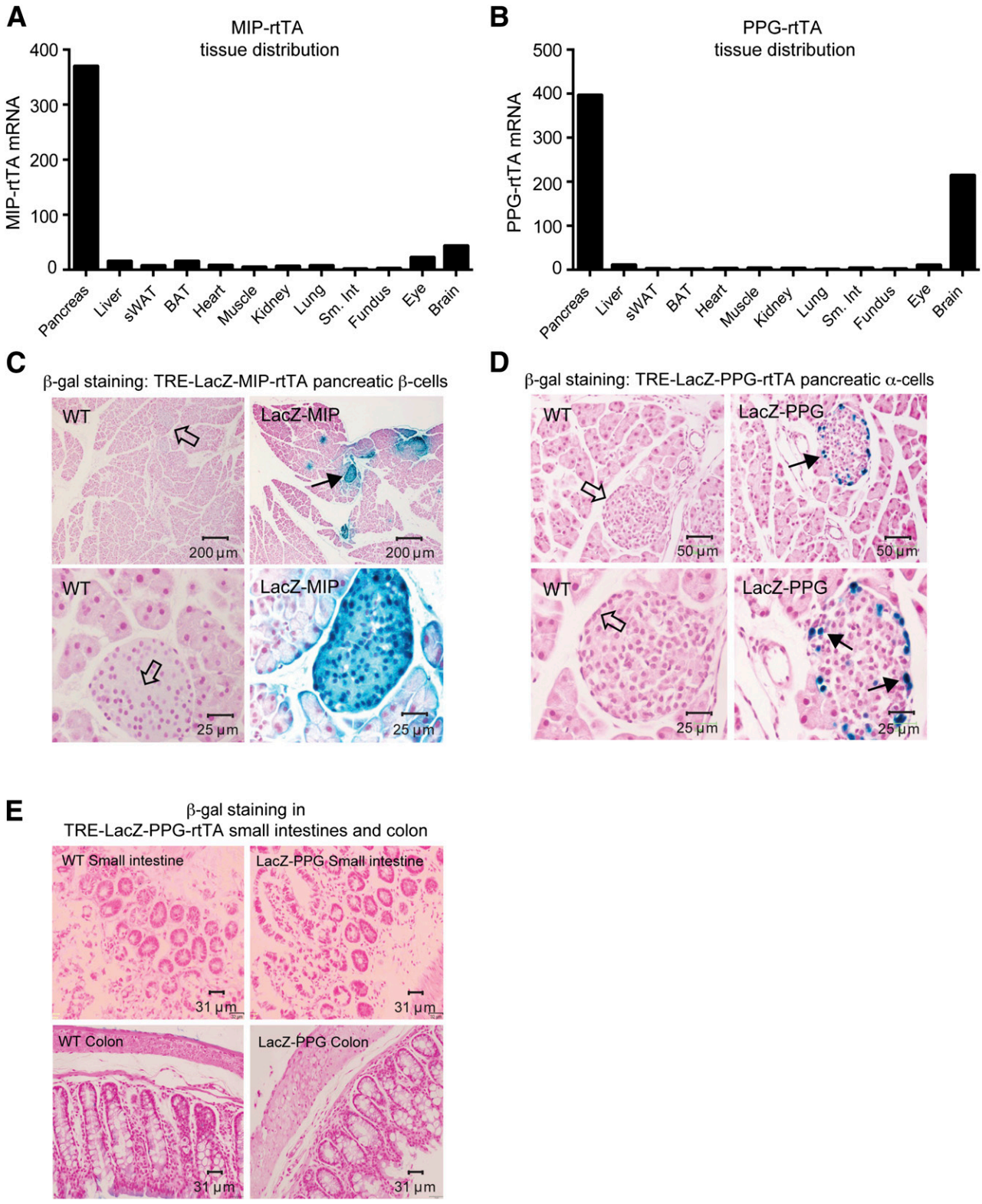

Figure 1—Generation and validation of *MIP-rtTA* and *PPG-rtTA* mice by using an inducible β-gal system. *A* and *B*: Representative tissue distributions of *MIP-rtTA* (*A*) and *PPG-rtTA* mRNA expression (*B*) in the pancreas, liver, subcutaneous (sWAT), brown adipose tissue (BAT), heart, skeletal muscle, kidney, lung, small intestine (Sm. Int), stomach fundus, eye, and whole-brain tissues derived from a male C57/BL6 *MIP-rtTA* mouse or a *PPG-rtTA* mouse after 1 week of Dox-chow (600 mg/kg) feeding. *C* and *D*: β-gal staining of pancreata derived from male C57/BL6 WT *TRE-LacZ-MIP-rtTA* (*LacZ-MIP*) (*C*) or *TRE-LacZ-PPG-rtTA (LacZ-PPG)* (*D*) mice after Dox-chow (600 mg/kg) feeding. Representative blue LacZ-positive β-gal staining is highlighted by solid arrows in centrally located β-cells within islets of *LacZ-MIP* pancreata (*C*) in addition to peripherally located α-cells in *LacZ-PPG* pancreata (*D*). Open arrows represent LacZ-negative β-cells and α-cells. *E*: A β-gal stain of L cells in small intestines and the colon of WT and *LacZ-PPG* mice after Dox-chow feeding.

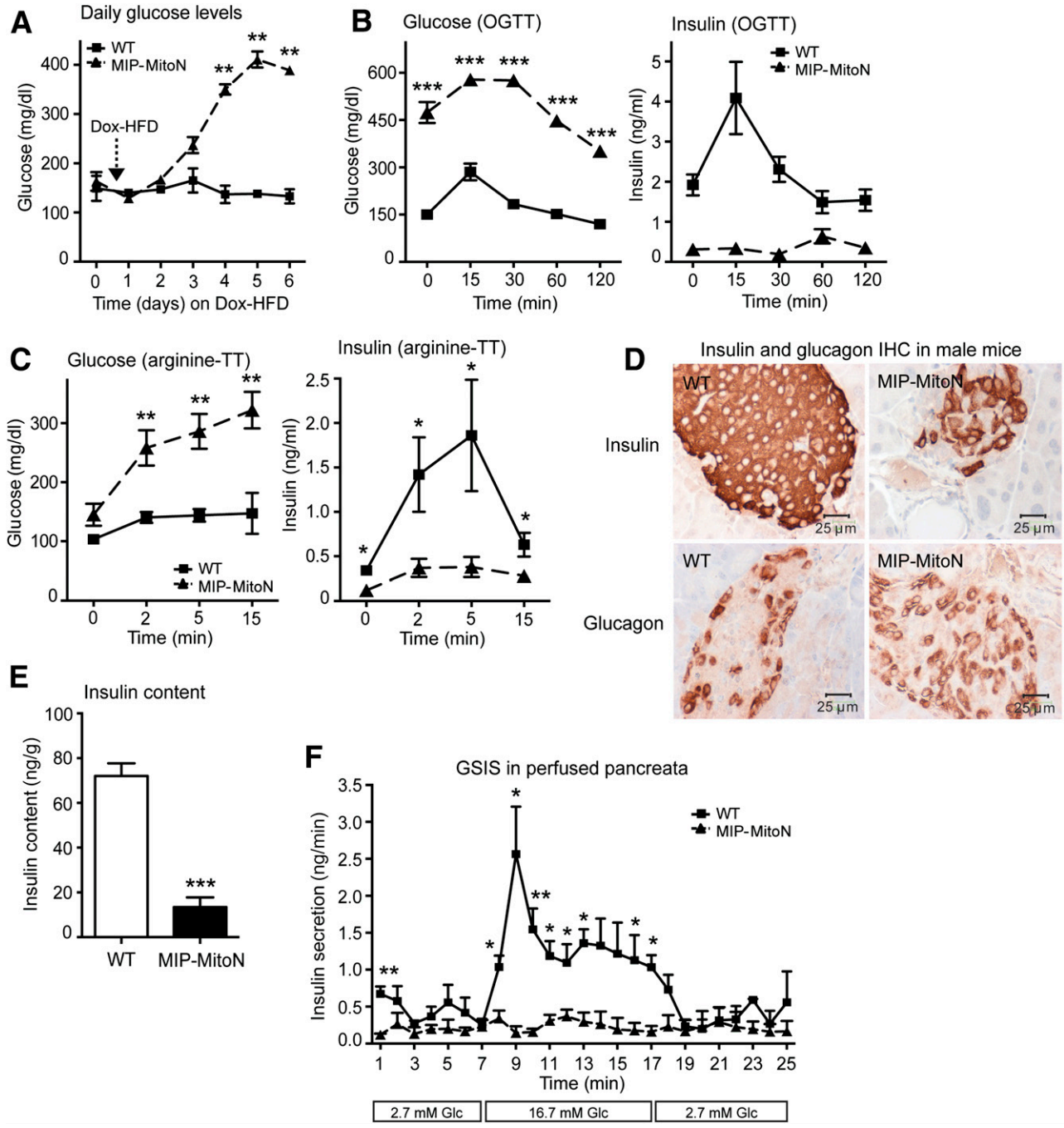

Figure 2— β-cell–specific MIP-MitoN mice exhibit hyperglycemia, glucose intolerance, β-cell dysfunction, and loss of β-cell mass. *A*: Daily ad libitum glucose levels in male C57/BL6 WT vs. *MIP-MitoN* mice during 6 days of Dox-HFD (600 mg/kg Dox) feeding (n = 6). Data are mean ± SEM. $^{**}P < 0.01$. *B*: Glucose levels (left) and insulin levels (right) during an OGTT (2.5 g/kg BW by gastric gavage following a 3-h fast) on male WT vs. *MIP-MitoN* mice (n = 5). $^{***}P < 0.001$. *C*: Glucose levels (left) and insulin levels (right) during an arginine tolerance test (TT) on male WT vs. *MIP-MitoN* mice fed Dox-HFD for 6 days. Mice were fasted (14–16 h) before intraperitoneal injection of L-arginine (1 mg/g BW) (n = 5). $^{*}P < 0.05$, $^{**}P < 0.01$. *D*: Insulin (top) and glucagon (bottom) IHC staining on sectioned pancreata obtained from male WT vs. *MIP-MitoN* mice. *E*: Total pancreatic insulin content (ng/g) in WT vs. *MIP-MitoN* mice after Dox-HFD feeding (n = 8). $^{***}P < 0.001$. *F*: Insulin secretion rates (ng/min) during perfusion of pancreata in 600 mg/kg Dox-chow fed WT vs. *MIP-MitoN* mice. Pancreata were perfused with a low glucose concentration (2.7 mmol/L) for up to 7 min followed by a high glucose concentration (16.7 mmol/L) for up to 10 min and then again with a low glucose dose for up to 8 min (n = 3). $^{*}P < 0.05$, $^{**}P < 0.01$. *G*: Daily ad libitum glucose levels during 6 days of Dox-HFD (600 mg/kg) feeding of female WT vs. *MIP-MitoN* mice (n = 3). *H*: Insulin (top) and glucagon (bottom) IHC of female WT vs. *MIP-MitoN* pancreata on day 7 of Dox-HFD feeding. *I*: Daily ad libitum glucose levels during a Dox titration time course in male WT vs. *MIP-MitoN* mice during 7 days of Dox-chow (25, 50, or 100 mg/kg Dox) feeding (n = 6). $^{**}P < 0.01$. *J*: Glucose and insulin levels in male WT vs. *MIP-MitoN* mice during an OGTT (2.5 g/kg BW) following 7 days of 100 mg/kg Dox-chow (left) or 50 mg/kg Dox-chow (right) feeding (n = 6). $^{*}P < 0.05$, $^{**}P < 0.01$. Glc, glucose.

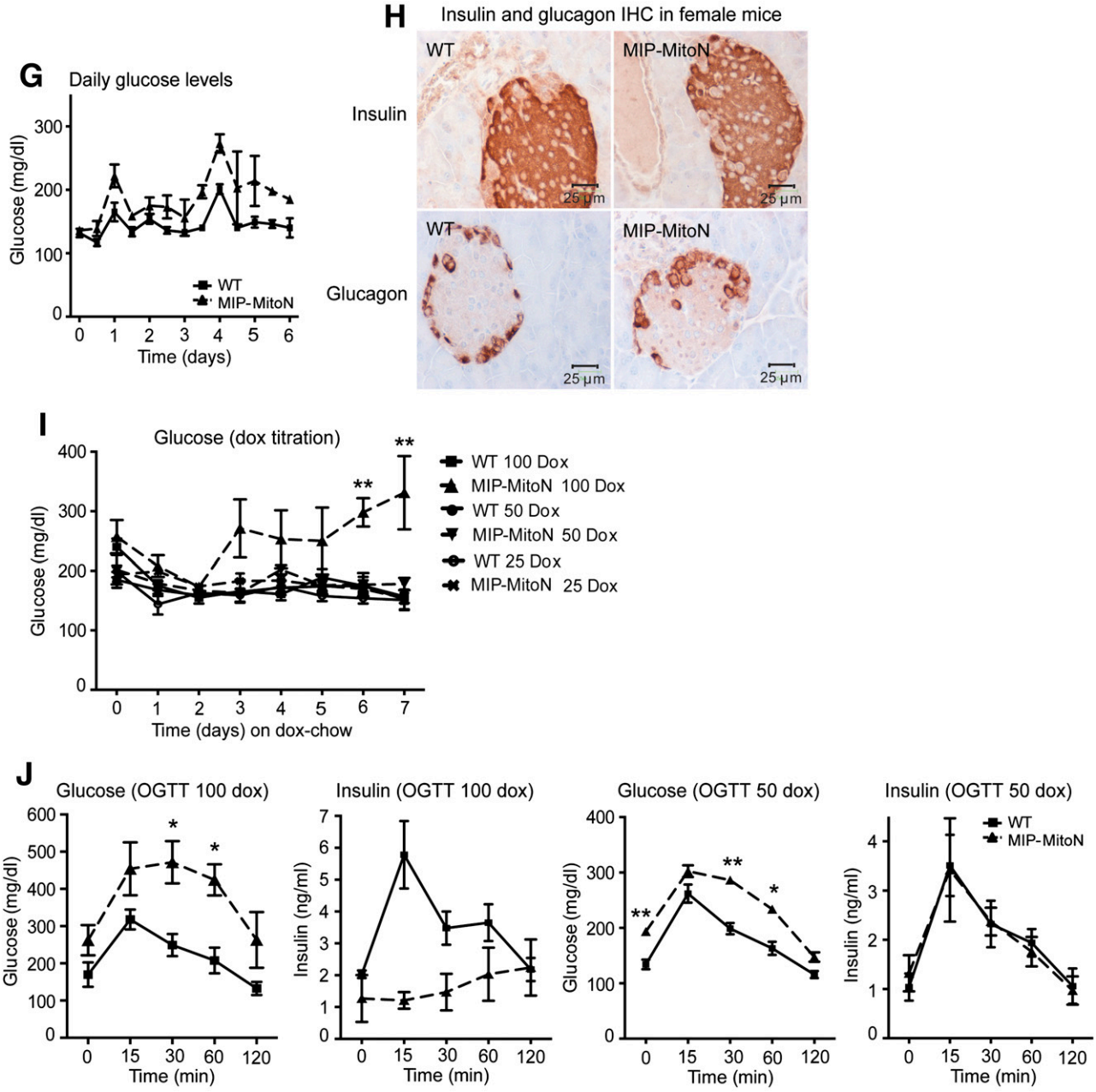

Figure 2—*Continued*.

Initial observations in *MIP-MitoN* mice were striking. After only 5 days of Dox-HFD feeding (600 mg/kg Dox), mice exhibited chronic hyperglycemia (Fig. 2*A*). *MIP-MitoN* mice were profoundly glucose intolerant, as demonstrated by diminished insulin secretion capacity during OGTT (Fig. 2*B*). An L-arginine tolerance test (an amino acid that stimulates the acutely releasable pool of insulin from β-cells) revealed that *MIP-MitoN* mice exhibited significantly impaired insulin release (Fig. 2*C*). IHC showed smaller-sized islets and less insulin-positive staining in β-cells, whereas α-cell glucagon signal remained intact (Fig. 2*D*). The system not only affects islet size but also islet numbers because quantitative analysis revealed an ∼50% reduction of islets in *MIP-MitoN* pancreata (WT mice 24 islets per tissue section, *MIP-MitoN* mice 14 islets). This was corroborated by significantly lower total pancreatic insulin content in *MIP-MitoN* mice, integrating the reduction of both size and number of islets per pancreas (Fig. 2*E*). Perfusing isolated pancreata with low followed by high concentrations of glucose to examine GSIS confirmed β-cell dysfunction in *MIP-MitoN* mice (Fig. 2*F*). Although WT mice responded with a classical glucose-induced biphasic insulin response consisting of a transient first phase with a longer second phase (29), *MIP-MitoN* mice completely lacked a response (Fig. 2*F*).

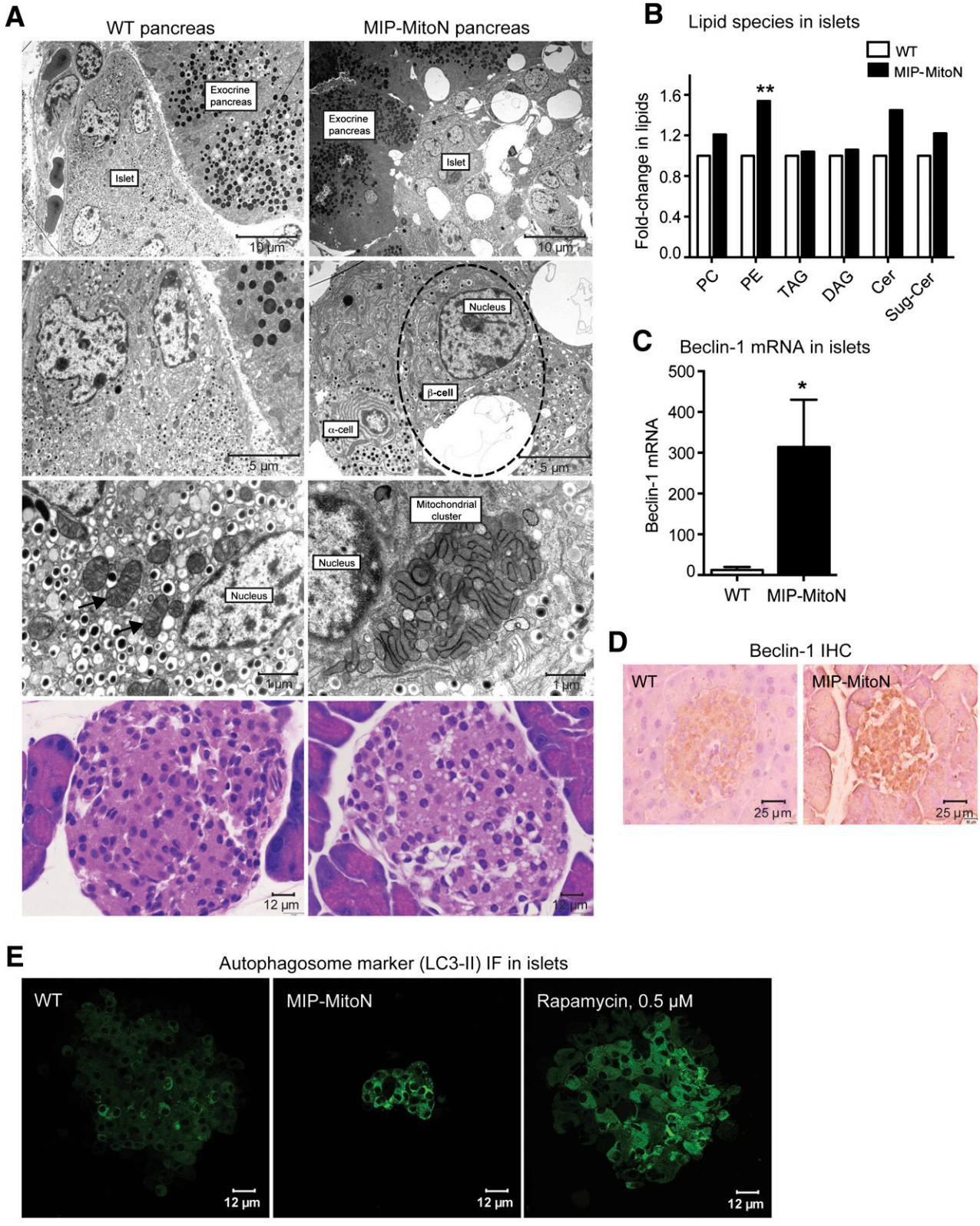

Figure 3—MitoNEET causes the formation of autophagic vacuoles and mitophagosomes in β-cells. *A*: Representative EM images of WT (left) and *MIP-MitoN* (right) pancreata from mice fed Dox-chow (100 mg/kg) for 2 weeks. The dashed outline highlights an *MIP-MitoN* β-cell containing an autophagic vacuole. The arrows point to WT β-cell mitochondria. The bottom panels show representative H-E staining of pancreata from WT and *MIP-MitoN* mice that underwent Dox-chow (100 mg/kg) feeding. *B*: Fold changes in lipid species content (phosphatidylcholine [PC], PE, triacylglycerol [TAG], diacylglycerol [DAG], ceramide [Cer], and sugar-ceramide [Sug-Cer] levels) in islets isolated from WT and *MIP-MitoN* mice after 2 weeks of Dox-chow (100 mg/kg) feeding ($n = 3$). Data are mean ± SEM. $^{**}P < 0.01$. *C*: Beclin-1 gene expression levels in islets isolated from WT and *MIP-MitoN* mice after 2 weeks of Dox-chow (100 mg/kg) feeding ($n = 5$). $^{*}P < 0.05$. *D*: Beclin-1 IHC in pancreata from WT and *MIP-MitoN* mice after 2 weeks of Dox-chow (100 mg/kg) feeding. *E*: Representative confocal

An interesting sexual dimorphism was noted in the present *MIP-MitoN* mice. Profound hyperglycemia was apparent in male *MIP-MitoN* mice during Dox-HFD feeding (Fig. 2*A*). Conversely, female *MIP-MitoN* mice are resistant to mitoNEET-driven hyperglycemia (Fig. 2*G*) and retain full insulin-positive β-cell mass (Fig. 2*H*) and islet numbers (WT females 25 islets, *MIP-MitoN* females 19 islets). This could be due to an inherently higher resistance to the negative consequences of compromised mitochondrial function. Although female *MIP-MitoN* mice induced mitoNEET ~2.5-fold in β-cells, overexpression was not as pronounced in male mice (Supplementary Fig. 3*A*). Nevertheless, a comparable fold induction in male *MIP-MitoN* mice still very effectively caused significant β-cell dysfunction, hyperglycemia, and glucose intolerance (Fig. 2*J*), suggesting that female mice are inherently more resistant to the effects of mitoNEET. Female mice also have higher circulating levels of adiponectin compared with male mice (30), and adiponectin-overexpressing mice display protection from β-cell apoptosis and diabetes (31). Female mice also display potent protection from caspase-8–mediated apoptosis (R.Y., P.E.S., unpublished observations). Future studies investigating how female *MIP-MitoN* mice cope with compromised mitochondrial function with ease and manage to sustain normoglycemia during a mitoNEET-driven β-cell insult should prove illuminating.

To examine the effects of mitoNEET on β-cell function without concomitant cellular death, we titrated the dose of Dox. Figure 2*I* shows that from a range of Dox concentrations (25, 50, or 100 mg/kg), the 100 mg/kg dose resulted in significantly higher glucose levels in *MIP-MitoN* mice. By using lower doses of Dox (50 or 100 mg/kg) in *MIP-MitoN* mice, glucose tolerance was impaired without associated hyperglycemia (Fig. 2*J*). This reflects the high level of reproducibility in the present mouse model, with a precisely titratable degree of β-cell dysfunction linked to an inducible diabetic readout. It further highlights the extremely high degree of sensitivity of the β-cell to an even slight reduction in mitochondrial perturbation.

MitoNEET Induction Forms Large Autophagic Vacuoles and Mitophagosomes in β-Cells Through Activation of Parkin-Dependent Mitophagy

Pancreatic β-cells harbor an interconnected filamentous network of mitochondria. However, when mitochondria become fused or fragmented, GSIS is impaired (6,32). By using electron microscopy (EM), we previously identified that WAT-specific induction of mitoNEET causes elongated, fused, and dysfunctional mitochondria (15). However, we did not observe any apoptotic adipocytes or aggregates. Here, EM of pancreata from 100 mg/kg Dox-chow fed mice was striking. *MIP-MitoN* islets displayed enlarged vacuoles that were restricted to the islet and not present in the exocrine pancreas or WT islets (Fig. 3*A*, first panel). Higher magnification revealed each *MIP-MitoN* β-cell to contain a single large vacuole, which was not evident in *MIP-MitoN* α-cells (Fig. 3*A*, second panel), highlighting a mitoNEET-driven β-cell–autonomous phenomenon. Vacuoles were not present in *MIP-MitoN* mice fed 600 mg/kg Dox-chow (data not shown), suggesting a dose-dependent effect of mitoNEET. Fewer insulin granules were evident in *MIP-MitoN* β-cells, whereas the numbers of glucagon granules appeared similar (Fig. 3*A*, second panel).

To assess whether the vacuoles in *MIP-MitoN* β-cells are lipid droplets, we quantified lipid species in islets from WT and *MIP-MitoN* mice fed 100 mg/kg Dox-chow. Although no marked differences in triacylglyceride or diacylglyceride levels were apparent, a significant increase in phosphatidylethanolamine (PE) levels, with a trend toward elevated levels of other membrane-associated lipid species (phosphatidylcholine, ceramides, and glycoceramides) was observed (Fig. 3*B*). However, the overall increase in lipid species did not account for the massive structure observed, suggesting that this may be a vacuolar organelle. Consistent with this, we were unable to stain islets with the neutral lipid stain oil red O (data not shown). A key reaction in autophagy entails the conjugation of the ubiquitin-like protein Atg8 to the lipid PE in autophagic membranes (33); levels of Atg8-PE conjugate correlate with autophagosomal size (34). We

images of IF staining by using the autophagosome marker LC3-II in islets isolated from WT and *MIP-MitoN* mice following 2 weeks of Dox-chow (100 mg/kg) feeding. *F*: *Park2* gene expression levels in islets isolated from WT and *MIP-MitoN* mice after 2 weeks of Dox-chow (100 mg/kg) feeding ($n = 5$). ***$P < 0.001$. *G*: Representative Western blots showing Parkin and mitoNEET protein expression levels in islets isolated from WT and *MIP-MitoN* mice after 2 weeks of Dox-chow (100 mg/kg) feeding. Bar graphs show Parkin and mitoNEET levels normalized to β-actin. Of note, the ectopically expressed mitoNEET is carboxy-terminally FLAG-tagged, giving rise to a slightly slower migrating band by Western blotting, with the faster migrating band corresponding to endogenous mitoNEET present in both WT and transgenic cells. *H*: Western blot showing mitoNEET protein expression levels in islets isolated from WT and *MIP-MitoN* mice after 2 weeks of Dox-chow (100 mg/kg) feeding. *I*: Daily ad libitum glucose levels in WT, *MIP-MitoN*, *Park-KO*, and *Park-KO-MIP-MitoNEET* (*Park-KO-MitoN*) mice during Dox-chow (600 mg/kg) feeding for 7 days ($n = 7$). *$P < 0.05$, **$P < 0.01$, ***$P < 0.001$. *J*: Glucose and insulin levels in *WT*, *MIP-MitoN*, *Park-KO*, and *Park-KO-MitoN* mice during an OGTT performed after 1 week of Dox-chow (600 mg/kg) feeding ($n = 6$). *K*: Representative EM images of WT, *Park-KO*, *MIP-MitoN*, and *Park-KO-MitoN* pancreata from mice fed Dox-chow (100 mg/kg) for 2 weeks. *L*: Representative confocal microscopy images of INS-1 β-cells transfected with CMV-mitoNEET-IRES-GFP plasmid and stained with the $\Delta\Psi_m$ dye TMRM. The dashed outlines highlight the cells of interest that overexpress mitoNEET. *M*: Representative confocal microscopy images of INS-1 β-cells transfected with CMV-mitoNEET-IRES-GFP plasmid (top) or CMV-GFP plasmid (bottom) stained with TMRM. The dashed outlines highlight the cells of interest that overexpress mitoNEET. The yellow arrow indicates the midstages of small mitophagosome formation with moderate mitoNEET induction. The white arrows highlight late-stage large mitophagosome formation with chronic mitoNEET induction. FCCP, carbonyl cyanide-4-phenylhydrazone.

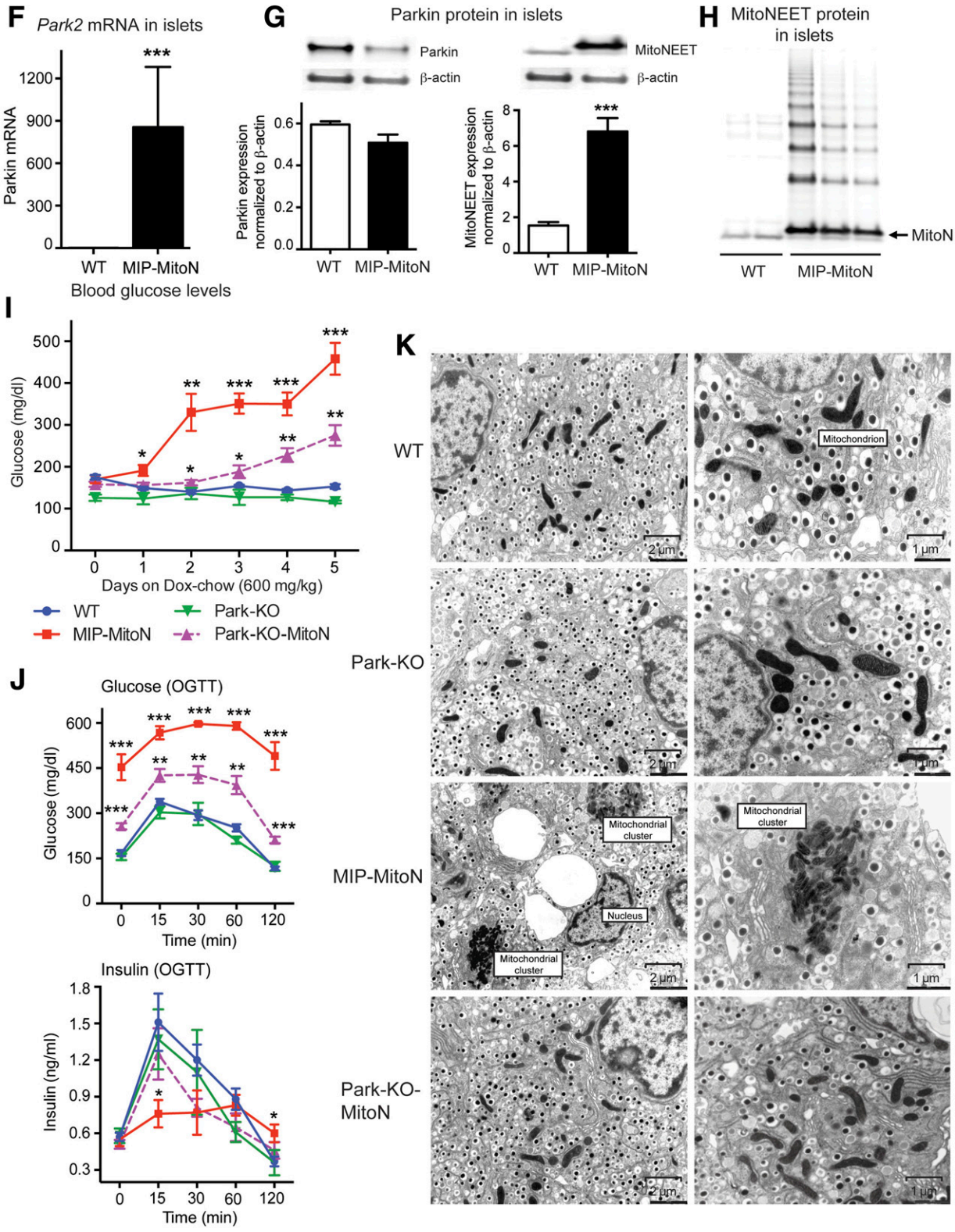

Figure 3—*Continued*.

therefore suggest that the structures present in *MIP-MitoN* β-cells are autophagic vacuoles targeted for lysosomal degradation. Although WT islet mitochondria exhibit a classical mitochondrial shape with clearly visible cristae (35), conversely, *MIP-MitoN* islets harbor numerous abnormally shaped mitochondrial clusters (comparable in size to the diameter of the nucleus) that exhibit undefined cristae (Fig. 3*A*, third panel). Mitochondrial cluster

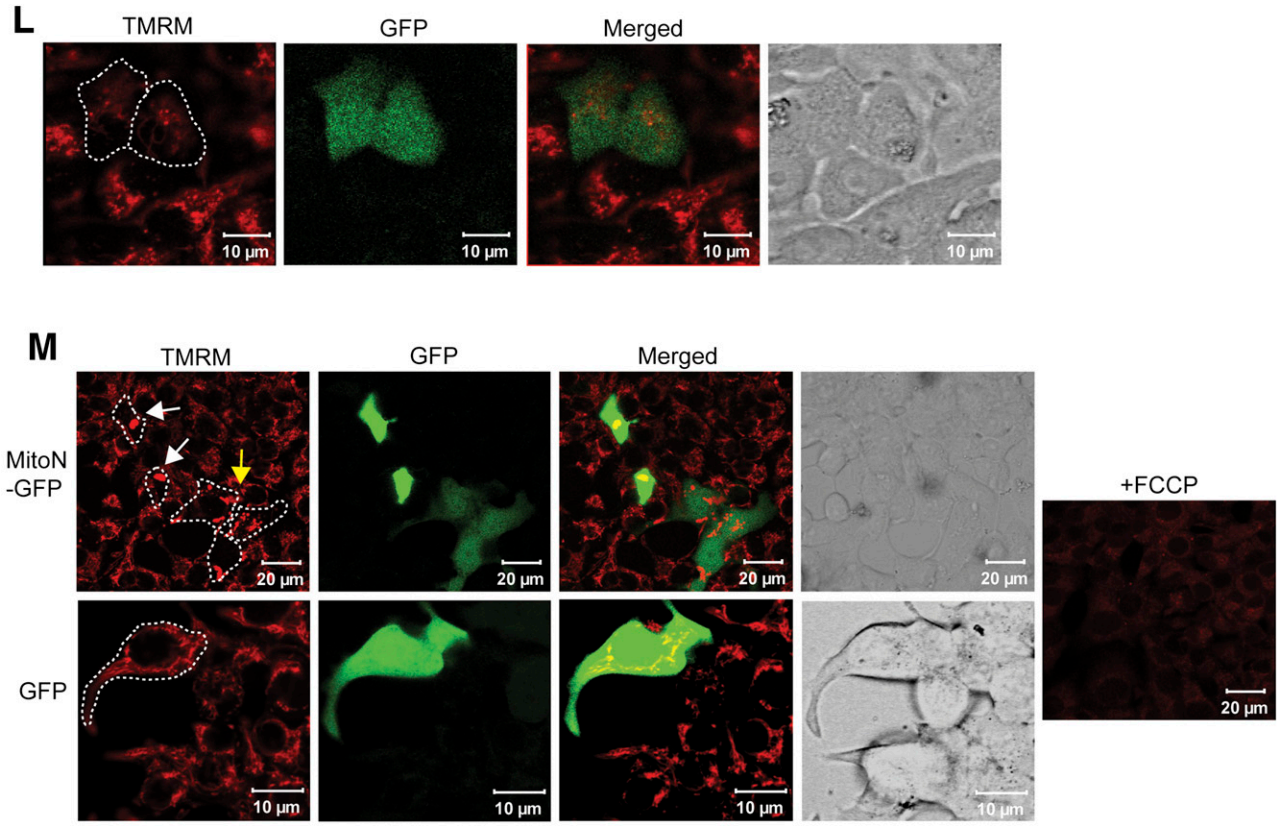

Figure 3—*Continued*.

formation (although not to the same extent) has been reported in β-cells in which autophagy is activated by exposure of the cells to palmitate (36). In the current study, mitoNEET may have promoted mitophagy and/or mitophagosomal accumulation. H-E staining confirmed the presence of the large vacuolar structures in *MIP-MitoN* islets that were apparent through EM (Fig. 3*A*, fourth panel).

Autophagy is a lysosomal degradation pathway essential for cell survival that is a critical compensatory response to numerous insults (37). In the current study, beclin-1 levels, an established marker of autophagy (38), were significantly upregulated in *MIP-MitoN* islets (Fig. 3*C* and 3*D*). Similarly, LC3-II, a marker of autophagosomes (39), revealed higher LC3-II–positive autophagic activity in *MIP-MitoN* islets on par with positive-control rapamycin-treated islets (Fig. 3*E*). Low-dose mitoNEET induction in β-cells, therefore, activates a critical autophagic pathway that forms unique mitophagosomes in β-cells hitherto never observed to this extent in the pancreas.

Parkin is an E3 ubiquitin-protein ligase that together with PTEN-induced putative kinase 1 (PINK1) orchestrates a mitochondrial quality control system to promote cellular survival through autophagy of damaged mitochondria, a process termed mitophagy (40,41). A single nucleotide polymorphism highlighted the *Park2* gene as a candidate susceptibility gene for diabetes that plays a role in β-cell insulin secretion (42). Several studies corroborate a Parkin-mediated mitophagy pathway in β-cells (43), and in HeLa cells, Parkin polyubiquitinates mitoNEET on the OMM (44). Here, a massive transcriptional upregulation of Parkin was evident in *MIP-MitoN* islets (Fig. 3*F*). Conversely, we were surprised to observe a moderate reduction in Parkin protein expression in transgenic islets (Fig. 3*G*). Such disconnect between transcriptional and posttranslational mechanisms that mediate Parkin expression in *MIP-MitoN* islets suggests either destabilization of the mitochondrial architecture and/or self-ubiquitinated proteasomal-mediated degradation of Parkin on the OMM, the latter a phenomenon that regulates Parkin degradation rates (45). Given the reduction in protein levels, Parkin may undergo rapid proteolysis postrecruitment to the OMM; the system may compensate through transcriptional upregulation in *PARK2* message. MitoNEET may serve as one of the substrates for Parkin-mediated ubiquitination. Western blotting for mitoNEET in transgenic islets implicated extensive ladder formation, consistent with the addition of a number of 8.5-kDa ubiquitin chains (Fig. 3*H*). Of note, mitoNEET contains 13 lysine residues, and blotting revealed a minimum of nine distinct mitoNEET bands with the potential to have additional, unresolved populations at higher molecular weights.

To test our hypothesis that mitoNEET functions through a Parkin-dependent mechanism, we crossed *MIP-MitoN* mice with *Park-KO* mice. Although *MIP-MitoN* mice exhibited chronic hyperglycemia within only a few

days of Dox-chow feeding (600 mg/kg), *MIP-MitoN* mice lacking Parkin (*Park-KO-MitoN* mice) displayed significantly lower glucose levels (Fig. 3*I*) and were at least partially protected from glucose intolerance (Fig. 3*J*). Of note, mitoNEET transgene levels upregulated regardless of a Parkin knockout (Supplementary Fig. 3*C*), indicating no inhibition of transgene expression in the absence of Parkin. We also confirmed that no defects in insulin secretion are evident in *Park-KO* mice (Fig. 3*J*). Although mitophagosomes and enlarged vacuoles were present in *MIP-MitoN* pancreata, no such structures were evident in *Park-KO-MitoN* pancreata (Fig. 3*K*). After transfection of INS-1 β-cells with either a CMV-mitoNEET-IRES-GFP plasmid or a control CMV-GFP plasmid, we observed a mitoNEET-driven lowering of $\Delta\Psi_m$ in the early stages of mitoNEET induction (Fig. 3*L*), with large punctate mitophagosomal aggregates forming in the later stages of mitoNEET overexpression (Fig. 3*M*). Of note, no mitophagosomes were evident in cells transfected with CMV-GFP alone, highlighting a mitoNEET-specific effect (Fig. 3*M*).

Collectively, these observations point to a mechanism whereby Parkin-dependent mitophagy in β-cells causes β-cell dysfunction in *MIP-MitoN* mice. Therefore, the current model is similar to our previous observations in the adipocyte (15): In β-cells, mitoNEET lowers $\Delta\Psi_m$. A reduction in $\Delta\Psi_m$ recruits the PINK1-Parkin complex to mitochondria to activate mitophagy (46) (Fig. 7A). However, although Parkin ubiquitinates mitoNEET (47), and likely numerous other proteins, we do not know what the functional implications are for this ubiquitination reaction and whether this further stimulates mitophagy. Future studies examining the consequences of this ubiquitination should therefore prove illuminating.

Modes of Regenerating or Preserving β-Cell Mass and Function: The Impact of Thiazolidinediones

Inducing mitoNEET in β-cells causes cellular dysfunction and loss of β-cell mass. We evaluated whether β-cells can regenerate and/or exhibit a full functional recovery after a mitoNEET-driven insult. If so, would an improvement in whole-body glucose tolerance ensue? *MIP-MitoN* mice were fed high-dose Dox-HFD (600 mg/kg) for 1 week. To lower mitoNEET levels and minimize HFD-induced insulin resistance, mice were switched to a non–Dox-containing chow diet to allow recovery and/or potential regeneration of β-cells postinjury. Upon reverting back to chow diet, *MIP-MitoN* mice achieved almost normoglycemia within 2–3 weeks after mitoNEET insult (Fig. 4*A*). The restoration of islet numbers (WT 33 islets; *MIP-MitoN* 33 islets) and insulin-positive signal (Fig. 4*B*) suggests recovery of β-cell mass. However, β-cell functionality was not entirely restored. Despite near-euglycemic glucose levels and the ability to mount an insulin response to glucose challenge, persistent glucose intolerance in *MIP-MitoN* mice was evident (Fig. 4*C*).

Thiazolidinediones (TZDs) are agonists for nuclear PPARγ that enhance insulin sensitivity in patients with diabetes (48). In β-cells, TZDs exert β-cytoprotective effects by preserving β-cell mass and islet architecture in a diabetic setting (49–51). We previously reported that treatment of PANIC-ATTAC mice (an inducible mouse model of β-cell loss and hyperglycemia) with a PPARγ agonist restores normoglycemia, improves glucose tolerance, and leads to the rapid regain of β-cell mass (51). Given that PANIC-ATTAC mice and *MIP-MitoN* mice share similarities in terms of β-cell dysfunction, β-cell loss, and subsequent recovery of β-cell mass, we hypothesized that TZDs exert β-cell protection in a similar manner as in *MIP-MitoN* mice to PANIC-ATTAC mice. WT and *MIP-MitoN* mice were therefore fed Dox-chow (600 mg/kg Dox) or Pio-containing Dox-chow (40 mg/kg day Pio and 600 mg/kg Dox). *MIP-MitoN* mice fed Dox-chow alone exhibited the expected gradual hyperglycemia; however, *MIP-MitoN* mice fed Pio-containing Dox-chow were completely protected from mitoNEET-induced hyperglycemia (Fig. 4*D*). IHC for insulin and glucagon revealed that Pio preserves islet morphology and β-cell mass, as demonstrated by dense insulin staining in *MIP-MitoN* Pio-treated islets (Fig. 4*E*). Supplementary Fig. 3*B* shows that mitoNEET transgene levels are significantly upregulated in *MIP-MitoN* pancreata both in the absence and in the presence of Pio, confirming that the ability of Pio to maintain normoglycemia in *MIP-MitoN* mice is not a consequence of transgene suppression. TZDs, therefore, provide potent β-cytoprotective effects from mitoNEET-induced mitochondrial dysfunction and the ensuing β-cell loss.

An α-Cell–Specific Induction of MitoNEET Perturbs Local Glucagon Homeostasis and Causes Fasting-Induced Hypoglycemia and Hypersecretion of Insulin

Targeting the diabetogenic role of α-cells is becoming increasingly important in diabetes research (20). Suppression of glucagon may offer valuable therapeutic avenues. Manipulating mitochondrial function to curb α-cell–derived hyperglucagonemia in an obese and/or diabetic setting is a novel and hitherto unexplored area for the modification of α-cell physiology. The precise mechanisms by which mitochondria influence α-cell glucagon secretion remain to be established.

To induce mitoNEET in α-cells, *TRE-MitoN* mice were crossed with *PPG-rtTA* mice (Supplementary Fig. 2*B*). No marked differences in glucose tolerance were observed after 3 weeks of Dox-HFD (600 mg/kg) feeding (data not shown). However, *PPG-MitoN* mice exhibited fasting-induced hypoglycemia complemented by significantly higher insulin levels (Fig. 5*A*). Perfusing pancreata with low and then high concentrations of glucose to assess GSIS revealed hypersecretion of insulin from *PPG-MitoN* islets, with a profound insulin spike evident in the transient first phase of insulin release followed by significantly higher insulin levels in the prolonged second phase (Fig. 5*B*). IHC showed some loss of glucagon-positive signal in α-cells of *PPG-MitoN* islets (Fig. 5*C*, top and middle panels), with no difference in insulin staining apparent between WT and *PPG-MitoN* pancreata (Fig. 5*C*, bottom

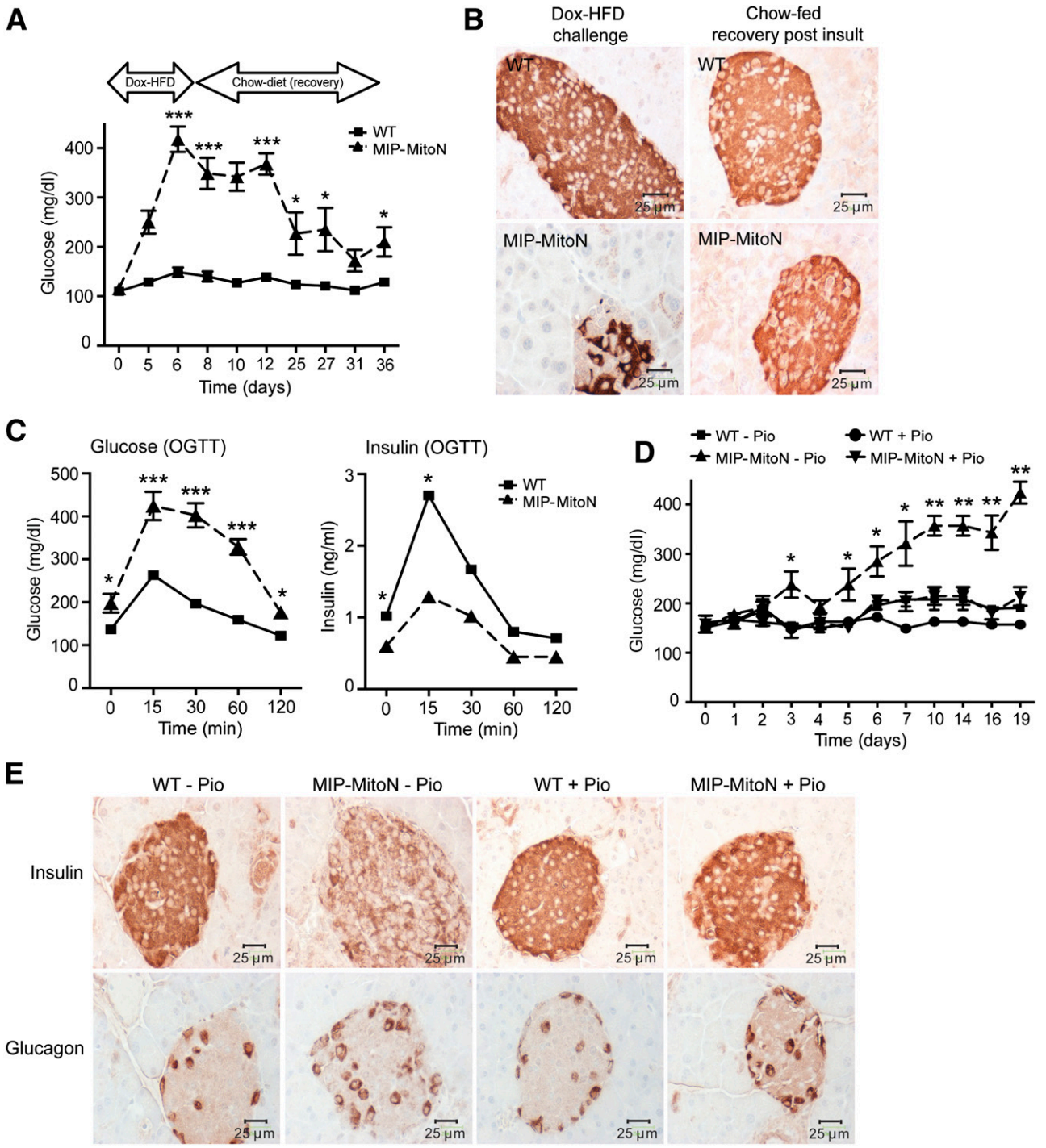

Figure 4—Regeneration of β-cell mass in *MIP-MitoN* mice after mitoNEET-induced insult but minimal recovery of β-cell functionality. *A*: Glucose levels in WT vs. *MIP-MitoN* mice during Dox-HFD (600 mg/kg) feeding for 1 week then postrecovery (standard chow diet feeding) for 4 weeks ($n = 5$). Data are mean ± SEM. $^{*}P < 0.05$, $^{***}P < 0.001$. *B*: Insulin IHC in WT vs. *MIP-MitoN* pancreata after Dox-HFD challenge (600 mg/kg) and after chow feeding (the recovery stage). *C*: Glucose and insulin levels in WT vs. *MIP-MitoN* mice during an OGTT during the recovery chow diet feeding stage (3 weeks after the initial Dox-HFD mitoNEET-induced insult) ($n = 5$). $^{*}P < 0.05$, $^{***}P < 0.001$. *D*: Daily ad libitum glucose levels in WT vs. *MIP-MitoN* mice during feeding of Dox-chow (600 mg/kg) either with the TZD Pio (40 mg/kg/day) or without Pio ($n = 5$). $^{*}P < 0.05$, $^{**}P < 0.01$. *E*: Insulin and glucagon IHC staining of pancreata from WT vs. *MIP-MitoN* mice fed either Dox-chow (600 mg/kg) alone (−Pio), or Pio-containing Dox-chow (+Pio).

panel). Although EM revealed a relatively normal cellular architecture in *PPG-MitoN* α-cells (Fig. 5*D*, top panel), mitophagosomes were evident (Fig. 5*D*, bottom panel) similar to those in *MIP-MitoN* β-cells (Fig. 3*A*). This implies that mitoNEET-induced mitochondrial dysfunction activates mitophagy in the α-cell, forming large mitophagosomes

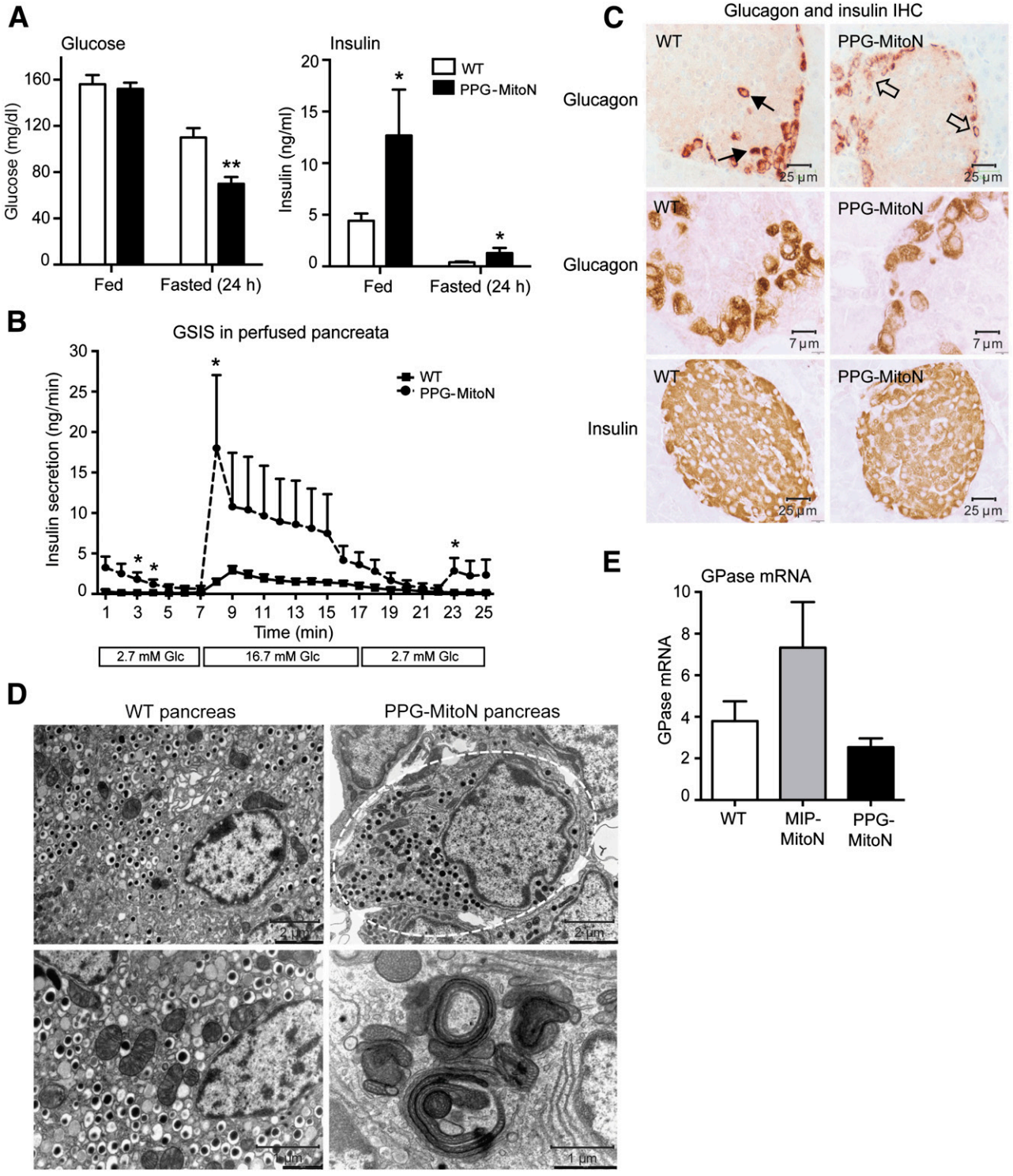

Figure 5—Enrichment of mitoNEET in α-cells results in fasting-induced hypoglycemia, hypersecretion of insulin during GSIS, and low glucagon–positive signal in islets. *A*: Ad libitum and fasted (24 h) glucose and insulin levels in male C57/BL6 WT vs. *PPG-MitoN* mice after 2 weeks of Dox-HFD (600 mg/kg) feeding ($n = 4$). Data are mean ± SEM. *$P < 0.05$, **$P < 0.01$. *B*: Insulin secretion rates (ng/min) during perfusion of pancreata of Dox-HFD (600 mg/kg)–fed WT and *PPG-MitoN* mice. Pancreata were perfused with a low glucose dose (2.7 mmol/L glucose) for up to 7 min followed by a high glucose dose (16.7 mmol/L glucose) for up to 10 min and then again with a low glucose dose for up to 8 min ($n = 3$). *$P < 0.05$. *C*: IHC staining of glucagon (top and middle panels, with the middle panel showing a higher resolution image) in addition to insulin IHC (bottom panel) in pancreata derived from WT vs. *PPG-MitoN* mice fed Dox-HFD (600 mg/kg) for 3 weeks. Solid arrows point to normal glucagon expression in α-cells in WT pancreata, whereas open arrows indicate loss of glucagon-positive staining in *PPG-MitoN* α-cells. *D*: Representative EM images of WT and *PPG-MitoN* pancreata from mice fed Dox-HFD (600 mg/kg) for 3 weeks. The dashed outline highlights glucagon granules within one α-cell. Scale bars indicate the resolution at which each image was taken. *E*: Hepatic glucose-6-phosphatase (GPase) gene expression levels after a 24-h fast in WT, *MIP-MitoN*, and *PPG-MitoN* mice after 3 weeks of Dox-HFD (600 mg/kg) feeding ($n = 4$). Glc, glucose.

similar to that in the β-cell. Consistent with local dysregulation in glucagon homeostasis, we observed a trend toward downregulation in downstream hepatic glucagon signaling targets of gluconeogenesis in *PPG-MitoN* mice. Glucose-6-phosphatase gene expression levels were moderately lower in *PPG-MitoN* livers after a 24-h fast; however, the differences did not reach statistical significance (Fig. 5*E*). *PPG-MitoN* mice, therefore, exhibit perturbed local glucagon signaling, with a disruption in islet homeostasis, as evidenced by dysinhibited secretion of insulin during GSIS.

Simultaneous Induction of MitoNEET in Both β-Cells and α-Cells Preserves β-Cell Viability Through Upregulation of Antiapoptotic Factors

MitoNEET promotes β-cell dysfunction and lowers α-cell glucagon production when overexpressed in each cell type individually. We therefore asked whether simultaneous mitoNEET-driven perturbation of both β-cells and α-cells would disrupt whole-islet homeostasis. To achieve this, *MIP-MitoN* mice were crossed with *PPG-MitoN* mice. Supplementary Fig. 2*G* confirms that we achieved sufficient induction of mitoNEET in *MIP-PPG-MitoN* pancreata after Dox-HFD feeding. Although *MIP-MitoN* mice (β-cells only) exhibited chronic hyperglycemia after only 5 days of Dox-HFD (Fig. 6*A*), *MIP-PPG-MitoN* littermates (both β-cell and α-cell induction of mitoNEET) retained normoglycemia (Fig. 6*A*). This finding suggests that dual overexpression of mitoNEET in both β-cells and α-cells is protective against the mitoNEET-driven β-cell dysfunction typically observed when mitoNEET is induced in β-cells alone. Consistent with this, 24-h fasting glucose levels confirmed hyperglycemia in β-cell–specific *MIP-MitoN* mice, significant hypoglycemia in α-cell–specific *PPG-MitoN* mice, but normoglycemia in α- and β-cell–specific *MIP-PPG-MitoN* mice (Supplementary Table 1). Although *MIP-MitoN* mice exhibited markedly lower insulin levels (Supplementary Table 1) due to loss of β-cell mass (Fig. 2*E* and 2*F*), their *PPG-MitoN* and *MIP-PPG-MitoN* littermates displayed significantly higher levels of insulin (Supplementary Table 1), again suggesting uninhibited insulin secretion due to dysregulated glucagon homeostasis. In line with a diabetic phenotype, *MIP-MitoN* mice harbor elevated circulating levels of neutral lipids (Supplementary Table 1), whereas no differences were apparent in *PPG-MitoN* mice or *MIP-PPG-MitoN* mice. Although *MIP-MitoN* mice displayed the expected impairment in glucose tolerance, no differences were observed in *MIP-PPG-MitoN* and *PPG-MitoN* mice (Fig. 6*B*). *MIP-PPG-MitoN* and *PPG-MitoN* mice, however, exhibited higher levels of insulin in response to glucose load (Fig. 6*B*) consistent with an enhanced insulin secretion capacity. IHC showed comparable staining of insulin and glucagon between WT and *MIP-PPG-MitoN* pancreata (Fig. 6*C*), suggesting that the α-cell copes with mitochondrial dysfunction more effectively when the β-cell is challenged under similar conditions, and vice versa. Although fasting (24 h) glucagon levels were comparable between WT and *PPG-MitoN* mice after 1 week of Dox-HFD feeding, *MIP-MitoN* and *MIP-PPG-MitoN* mice displayed significantly lower glucagon levels (Fig. 6*D*). In *MIP-PPG-MitoN* pancreata, EM revealed the presence of mitophagosomes in β-cells but not in α-cells (Fig. 6*E*), indicating that under these conditions, the α-cell overcomes the challenge of mitochondrial perturbation, leading to the formation of mitophagic structures. Under the same conditions, the β-cells formed mitophagosomes, suggesting that the formation of the structure per se does not lead to cellular dysfunction and may in fact preserve it. Consistent with that, we observed at least in INS-1 cells that these mitophagosomes preserve $\Delta\Psi_m$ (Fig. 3*M*). Both *PPG-MitoN* mice (α-cells) and *MIP-PPG-MitoN* mice (β- and α-cells) exhibited compromised α-cell function, yet the net result prevented the loss of β-cell mass typically seen in *MIP-MitoN* mice, suggesting that α-cell perturbation may emanate a potent protective signal toward β-cells to preserve their viability. We therefore hypothesized that compromised α-cells release an antiapoptotic β-cytotrophic factor that acts locally to target juxtaposed stressed β-cells. To explore this hypothesis, we sought to identify a potential α-cell–derived β-cytotrophic candidate originating from mitoNEET-enriched α-cells. We crossed *TRE-GFP* mice with *PPG-MitoN* mice to achieve GFP-specific labeling of mitoNEET-abundant α-cells. By using FACS, we isolated GFP-labeled α-cells from *GFP-PPG-MitoN* islets versus control *GFP-PPG* islets and then performed microarray methodology to screen for potential α-cell–derived survival candidates. The most prominent genes upregulated by mitoNEET in α-cells were nerve growth factor α (*Ngfa*), protein disulfide isomerase (pancreatic) (*Pdip*), and trefoil factor 2 (*Tff2*) (Table 1). *Ngfa* and *Tff2* are critical trophic factors that help to maintain the survival of β-cells through antiapoptotic properties (52–54). The profound upregulation of these survival factors in metabolically challenged *PPG-MitoN* α-cells suggests their importance in sustaining β-cell viability in this mouse model. Future studies delineating the precise mechanisms of how this mitoNEET-driven upregulation in *Ngfa* and *Tff2* promotes β-cell survival in a mouse model with perturbed α-cell homeostasis (the *PPG-MitoN* mouse) should prove interesting.

MitoNEET Promotes Transcriptional Profile Reprogramming of an α-Cell Into a β-Cell–Like Status

Upon further analyses of the *PPG-MitoN* α-cell microarray, we observed a striking switch in transcriptional patterning of the transgenic α-cells. *PPG-MitoN* α-cells exhibited a marked downregulation in several α-cell–predominant genes (*Gcg*, *Ttr*, *Nkx2.2*, and *Isl1*) (Table 2). At the same time, a profound upregulation in numerous β-cell–specific genes (*Ins1*, *Glut2*, *Nkx6.1*, *Pdx1*, *Iapp*, *ZnT8*, *Chga*, *Ngn3*, and *Ptfa1*) was evident in the transgenic α-cells (Table 2), suggesting that a mitoNEET-induced perturbation in α-cell mitochondrial function not only preserves β-cell viability through the production of a β-cytotrophic factor, but also simultaneously promotes transcriptional conversion from an α-cell state into a more β-cell–like profile. However,

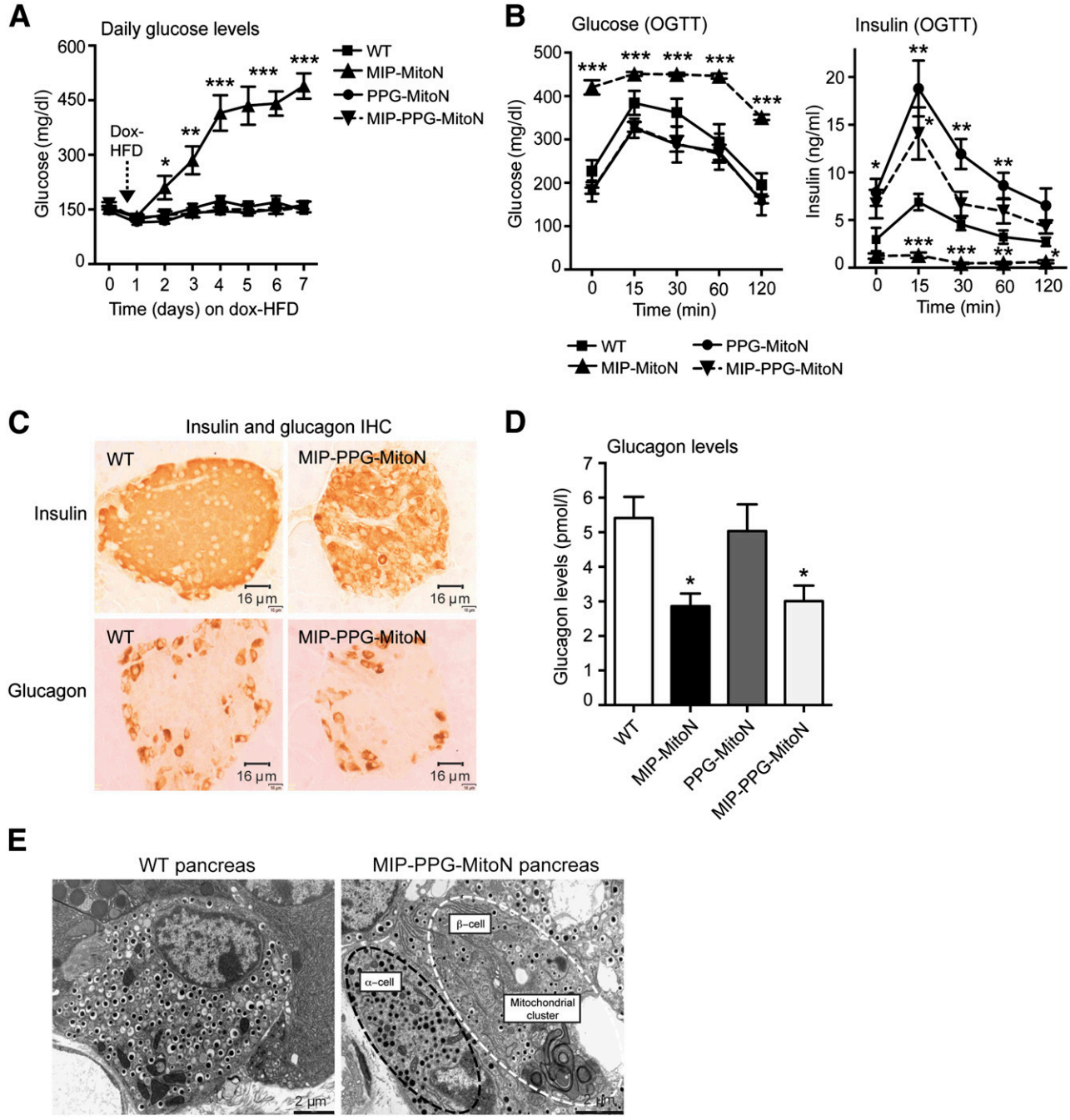

Figure 6—Dual induction of mitoNEET in both β-cells and α-cells protects mice from mitoNEET-driven hyperglycemia typically observed in β-cell–alone overexpressors. *A*: Daily ad libitum glucose levels in male C57/BL6 WT, *MIP-MitoN*, *PPG-MitoN*, and *MIP-PPG-MitoN* mice during 7 days of Dox-HFD (600 mg/kg) feeding (n = 6). *B*: Glucose and insulin levels during an OGTT in male WT, *MIP-MitoN*, *PPG-MitoN*, and *MIP-PPG-MitoN* mice (n = 6). Data are mean ± SEM. *P < 0.05, **P < 0.01, ***P < 0.001. *C*: IHC staining of insulin and glucagon in pancreata from WT vs. *MIP-PPG-MitoN* mice fed Dox-HFD (600 mg/kg). *D*: Circulating glucagon levels after a 24-h fast in WT, *MIP-MitoN*, *PPG-MitoN*, and *MIP-PPG-MitoN* mice after 1 week of Dox-HFD (600 mg/kg) feeding (n = 4). *E*: Representative EM images of WT and *MIP-PPG-MitoN* pancreata from mice fed Dox-HFD (600 mg/kg). The white outline highlights a β-cell, and the black outline highlights an α-cell.

complete rescue observed at the level of β-cell mass seems unlikely to be exclusively due to a conversion of α-cells. This can be inferred from the fact that many more β-cells than original α-cells remained present and that there did not appear to be a net depletion of α-cells converting to β-cells.

DISCUSSION

We generated and validated a novel mouse model that allows inducible cell-specific overexpression of any gene in pancreatic β-cells (the *MIP-rtTA* mouse). In conjunction, we also generated and characterized a novel α-cell–specific

Table 1—Top upregulated genes in α-cells isolated from *GFP-PPG-MitoN* pancreata

Gene	Gene definition	Fold-up	Function
Ngfa	Nerve growth factor, α	11.5	*Ngfa* is a critical trophic factor in maintaining the survival of β-cells; it exerts profound antiapoptotic and survival features. Pancreatic β-cells synthesize and secrete *Ngfa* to increase insulin production. Increased pancreatic *Ngfa* is an acute response of the pancreas to damage. *Ngfa* reduction activates β-cell apoptosis.
Pdip	Protein disulfide isomerase, pancreatic	7.1	A major intracellular storage protein that promotes the accumulation of pancreatic estrogen. Reported to provide strong protection to the cell against heat shock or oxidative stress–induced death. Estrogen is further known to protect β-cells from apoptosis and oxidative injury in addition to preventing insulin-deficient diabetes in mice.
Tff2	Trefoil factor 2	5.6	Antiapoptotic. Identified as a novel target for inducing β-cell proliferation. Promotes cell proliferation in β-cells through CXCR-4–mediated ERK1/2 phosphorylation.

Top genes identified by Illumina microarray that display the highest-fold upregulation in α-cells isolated from *TRE-GFP-PPG-rtTA* (*GFP-PPG*) pancreata (n = 4) vs. *TRE-MitoN-TRE-GFP-PPG-rtTA* (*GFP-PPG-MitoN*) pancreata (n = 7) from mice that underwent 2–3 weeks of Dox-HFD (600 mg/kg) feeding. Inclusion criteria were genes that are significantly altered more than fivefold in *GFP-PPG* α-cells vs. *GFP-PPG-MitoN* α-cells and exhibit an absolute value of >500 in abundance. Gene abbreviations, definitions, and fold alterations between *GFP-PPG* α-cells vs. *GFP-PPG-MitoN* α-cells are indicated.

mouse model (the *PPG-rtTA* mouse). We confirmed cell specificity in both mouse models by using an inducible TRE-LacZ labeling system in which positive β-gal signal is strictly confined to α-cells and β-cells, respectively. By utilizing the β-cell–specific *MIP-rtTA* mouse and exploiting the unique properties of the OMM protein mitoNEET to compromise mitochondrial function, we created a novel, inducible, and highly titratable mouse model of overt diabetes (the *MIP-MitoN* mouse). We demonstrate that male *MIP-MitoN* mice are profoundly hyperglycemic, are glucose and arginine intolerant, and exhibit low pancreatic insulin content due to widespread loss of β-cell mass. The severity of the β-cell insult can be tightly and effectively fine-tuned by careful titration of Dox administration, which at lower levels prompts β-cell dysfunction without resulting in β-cell loss. In vivo findings are corroborated by pancreatic perfusion experiments showing impaired GSIS in *MIP-MitoN* mice, with a complete lack in a first-phase insulin spike in response to glucose infusion. Mechanistically, low-dose mitoNEET induction activates Parkin-mediated mitophagy in β-cells, which leads to the formation of large vacuoles and mitophagosomes localized exclusively and specifically to each β-cell enriched with mitoNEET. Of note, this mechanism is reinforced by using *MIP-MitoN* mice null for

Table 2—MitoNEET promotes transcriptional reprogramming to drive an α-cell profile to a more β-cell conversion

Cell type–specific* gene	Gene definition	Fold change	Alteration
α-cell specific			
Gcg	Glucagon	1.8	↓
Ttr	Transthyretin	1.6	↓
Nkx2.2	NK2 homeobox 2	1.3	↓
Isl1	LIM homeodomain	1.3	↓
β-cell specific			
Ins1	Insulin I	2.2	↑
Ins2	Insulin II	1.0	—
Glut2	Facilitated glucose transporter, 2	4.0	↑
Nkx6.1	NK6 homeobox 1	2.2	↑
Pdx1	Pancreatic and duodenal homeobox 1	1.6	↑
Iapp	Islet amyloid polypeptide	2.1	↑
ZnT8	Solute carrier family 30 (Zn transporter), 8	1.3	↑
Chga	Chromagranin A	1.2	↑
Ngn3	Neurogenin 3	1.4	↑
Ptfa1	Pancreas-specific transcription factor 1a	5.0	↑
δ-cell specific			
Sst	Somatostatin	1.1	↓

Fold alterations in cell type–specific pancreatic genes identified by Illumina microarray analyses in α-cells isolated from *TRE-GFP-PPG-rtTA* (*GFP-PPG*) pancreata (n = 4) vs. *TRE-MitoN-TRE-GFP-PPG-rtTA* (*GFP-PPG-MitoN*) pancreata (n = 7) from mice that underwent 2–3 weeks of Dox-HFD (600 mg/kg) feeding. Gene abbreviations, definitions, and fold alterations between *GFP-PPG* α-cells and *GFP-PPG-MitoN* α-cells are indicated. *Known to be highly expressed in α-cells, β-cells, or δ-cells.

Parkin lacking any mitophagosomes in β-cells and exhibiting normoglycemia at the whole-body level. The TZD Pio, on the other hand, is protective against mitoNEET-driven hyperglycemia and prevents loss of β-cell mass. By removing Dox and thus restoring the physiological levels of mitoNEET, β-cells in *MIP-MitoN* mice regenerate to full mass. By using the *PPG-rtTA* mouse, we achieved induction of mitoNEET specifically in pancreatic α-cells. *PPG-MitoN* mice exhibited fasting-induced hypoglycemia as a result of an overproduction of insulin; this was substantiated by marked hypersecretion of insulin during glucose tolerance and GSIS. Such findings implicate mitoNEET-mediated dysregulation in local α-cell homeostasis, which likely unleashes uninhibited insulin secretion from the adjacent β-cell. By inducing mitoNEET in both β-cells and α-cells simultaneously, we rescued the β-cell dysfunction typically seen when mitoNEET is enriched in β-cells alone (i.e., double transgenic β-cell–α-cell *MIP-PPG-MitoN* mice retain normoglycemia despite their single transgenic β-cell–targeted *MIP-MitoN* littermates exhibiting severe hyperglycemia). This finding indicates that reduced mitochondrial function in α-cells is potently protective in terms of sustaining β-cell viability.

Efficient mitochondrial function is essential for the β-cell to exquisitely sense and translate available nutrient metabolites into signals to stimulate insulin secretion (55). Mitochondrial dysfunction, therefore, is a fundamental contributor to β-cell failure in diabetes (56), with defective mitochondria tightly coupled with blunted GSIS (57). In the current study, we present a unique *MIP-MitoN* mouse model of titratable mitochondrial impairment that can be used to examine the critical step-by-step stages from normal β-cell function to progressively impaired GSIS as a function of mitochondrial activity. The current mouse model also allows assessment of how β-cells protect themselves by unleashing compensatory mechanisms in response to incremental degrees of compromised mitochondrial function. Other means of compromising mitochondria in β-cells, such as hypoxia or chemical inhibition of the mitochondrial electron transport chain, severely impair GSIS or result in total ablation of β-cells (9,58,59), thus preventing the analyses of intermediate compensatory mechanisms. The titratable nature of the *MIP-MitoN* mouse provides a snapshot of the apparent transitional mechanisms by perturbing β-cell mitochondrial function, which may not be fully defined through more severe models of overt diabetes.

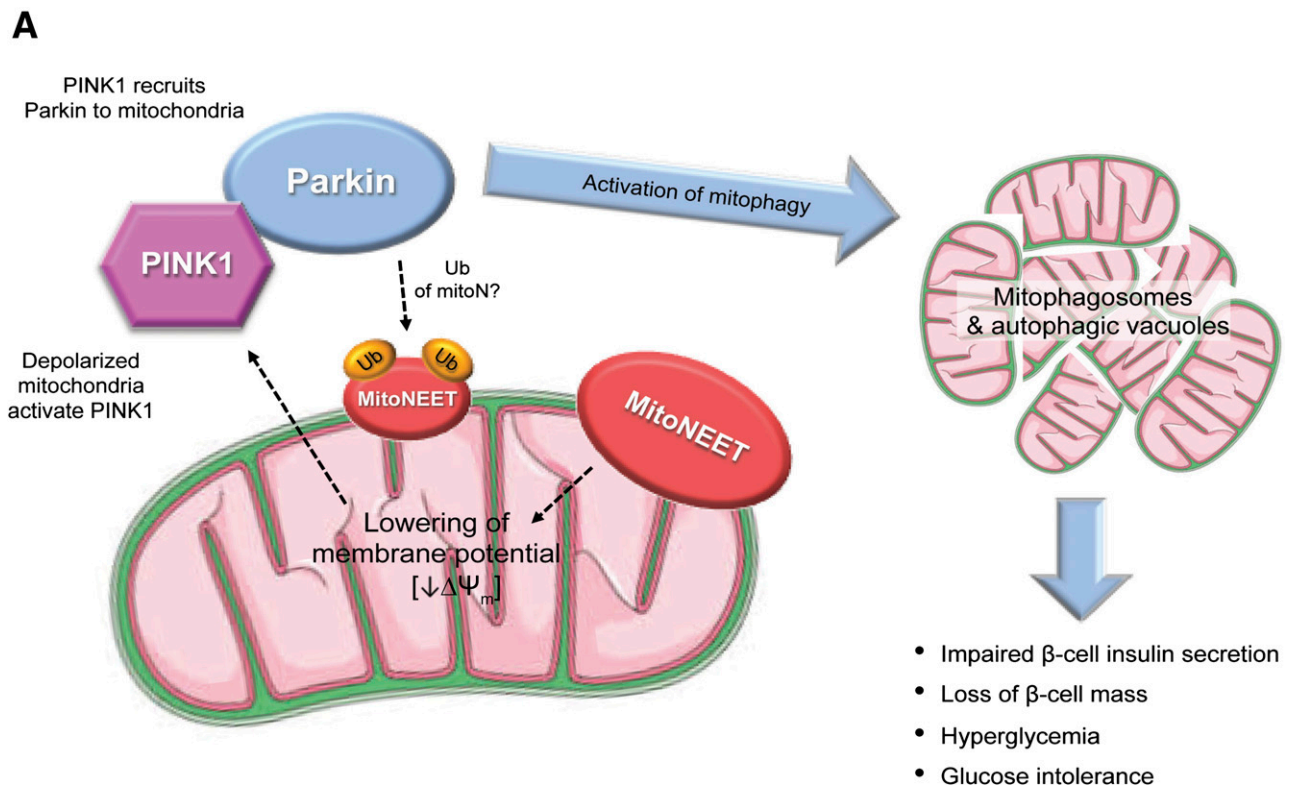

Figure 7—*A*: The mechanistic action of mitoNEET in *MIP-MitoN* β-cells. MitoNEET lowers $\Delta\Psi_m$. This depolarization of $\Delta\Psi_m$ activates PINK1 and recruitment of Parkin to the OMM to trigger mitophagy, as observed by the formation of mitophagosomes and autophagic vacuoles. Such effects impair the ability of the *MIP-MitoN* β-cell to secrete insulin and, under increasing concentrations of Dox, promote β-cell death. At the whole-body level, *MIP-MitoN* mice exhibit hyperglycemia and severe glucose intolerance. Parkin is also known to polyubiquitinate (Ub) mitoNEET; however, the functional implications of this modification are currently unknown. *B*: Proposed model of mitoNEET-driven cellular and whole-body action in *MIP-MitoN* mice (β-cell induction of mitoNEET), *PPG-MitoN* mice (α-cell induction), and *MIP-PPG-MitoN* mice (β- and α-cell induction).

Mitophagy, the selective autophagy of mitochondria, is associated with T2DM (60). Two proteins mediate the selective removal of defective mitochondria: the E3 ubiquitin-protein ligase Parkin acts in concert with the serine/threonine-protein kinase PINK1 (61). Both *PARK2* and *PINK1* are strong candidates as susceptibility genes associated with T2DM (62,63). In response to mitochondrial membrane depolarization, PINK1 recruits cytosolic Parkin to ubiquitinate proteins on the OMM (61,64); this induces LC3-II to form autophagosomes (65) and to trigger a mitophagic clearance system. In the current study, low-dose mitoNEET induction in β-cells caused large autophagic vacuoles to form within each *MIP-MitoN* β-cell; this is supported by an upregulation in beclin-1 levels and enhanced LC3-II activity in *MIP-MitoN* islets. MitoNEET also promotes the highly interconnected mitochondrial network within the β-cell body to collapse and form mitophagosomes. Collectively, the formation of autophagic vacuoles and mitophagosomes in *MIP-MitoN* β-cells is a direct consequence of mitoNEET activating an autophagic degradation pathway through a PINK1/Parkin- and beclin-1–dependent mechanism. Vives-Bauza et al. (64) reported that co-overexpression of PINK1 and Parkin in HEK293T cells causes overt alteration of the mitochondrial network by forming fragmented mitochondrial aggregates that undergo mitophagy, the latter confirmed by LC3-positive autophagic vacuoles. Of note, we previously identified that mitoNEET lowers $\Delta\Psi_m$ in adipocytes (15) and have

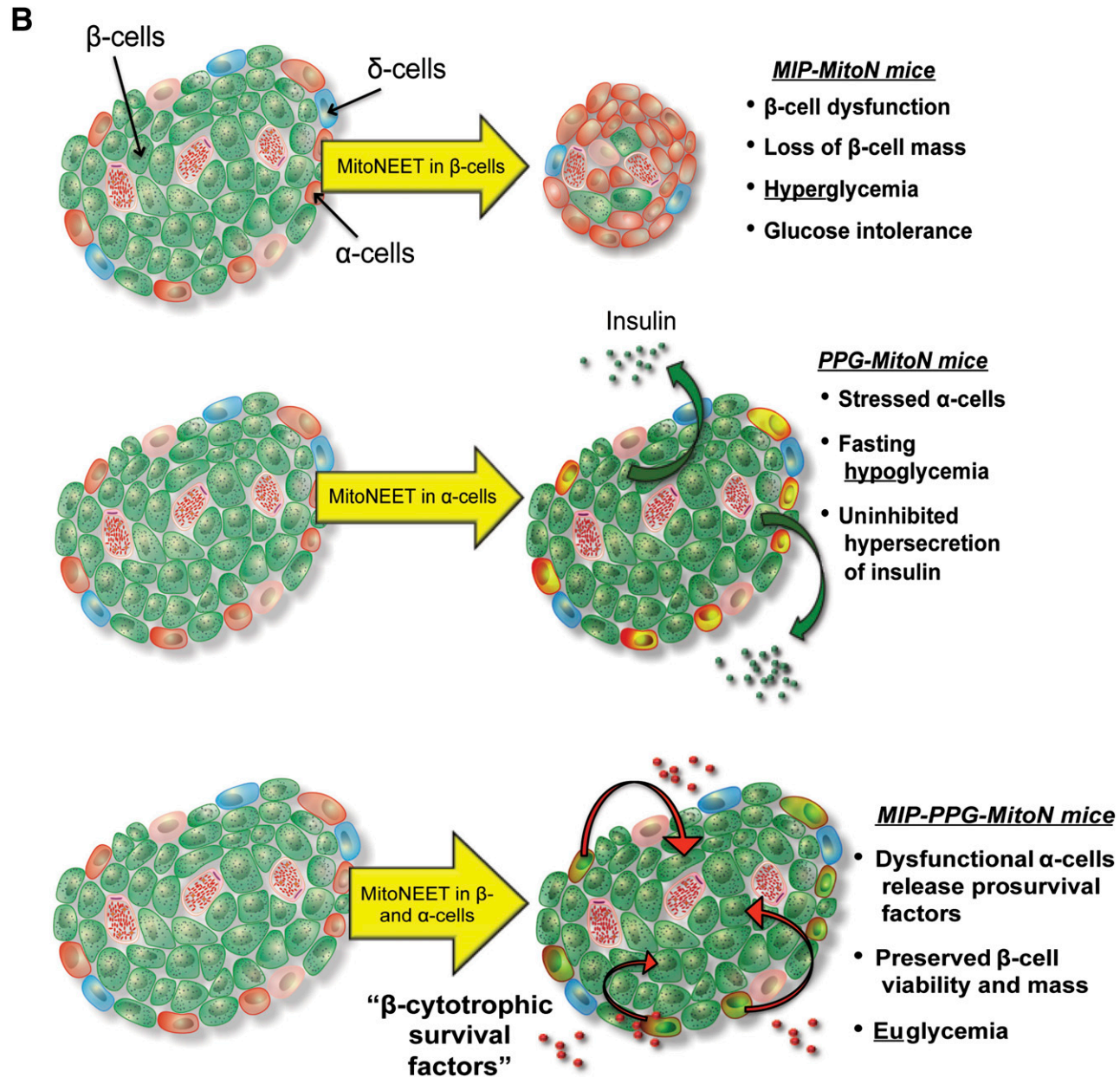

Figure 7—*Continued*.

confirmed this effect in β-cells in the present study. Furthermore, lowering $\Delta\Psi_m$ is perceived by the cell as mitochondrial damage (64). Given that loss of $\Delta\Psi_m$ activates PINK1 to relocalize Parkin to the OMM and trigger mitophagy (64), mechanistically, we propose that mitoNEET impairs mitochondrial function to lower the $\Delta\Psi_m$ and that this initiates a compensatory response by activating PINK1/Parkin-mediated mitophagy in an attempt to protect mitochondrial integrity (Fig. 7*A*). This mechanism was strengthened by data showing that *MIP-MitoN* mice that lack Parkin fail to form mitophagosomes and thus sustain normoglycemia. Finally, a Parkin-mitoNEET negative feedback loop may prime mitoNEET for degradation, as Lazarou et al. (47) identified mitoNEET as a direct substrate for polyubiquitination by Parkin on the OMM (Fig. 7*A*). This may explain the markedly lower mitoNEET expression levels observed in islets from leptin-deficient *ob/ob* mice (data not shown).

The intricate topographical architecture of α- and β-cells within the islet indicates coordinated reciprocal paracrine communication between the two cell types to achieve global glycemic stability. In the fed state, insulin suppresses glucagon to lower hepatic gluconeogenesis (66); vice versa during fasting, low insulin levels prompt a reciprocal increase in glucagon to stimulate hepatic glucose production. Coordination of these two hormones that diametrically oppose each other's action on hepatic fuel metabolism provides glycemic homeostasis. Glucagon, however, is a potent diabetogenic hormone such that a lack in local insulin availability to suppress glucagon release causes uncontrolled hyperglucagonemia, a major contributor to T2DM (66). Perturbing glucagon homeostasis could harbor therapeutic potential. The induction of mitoNEET in mature adipocytes effectively compromises mitochondrial function to alter cellular signaling (15). In the current study, we used mitoNEET as a genetic tool to impair α-cell mitochondrial function in the hope of disrupting glucagon homeostasis. *PPG-MitoN* mice exhibited fasting-induced hypoglycemia, a synergistic overproduction in insulin, and hypersecretion of insulin during GSIS. Indeed, impaired glucagon signaling unleashes uninhibited insulin secretion from β-cells (66).

Mice lacking proper glucagon signaling post streptozotocin-induced loss of β-cell mass do not develop diabetes (67,68). How can impaired glucagon signaling with complete β-cell loss equate to glycemic stability given that whole-islet signaling is compromised? To mimic this, we used mitoNEET to perturb α-cells and β-cells simultaneously to dysregulate the entire islet. Although *MIP-MitoN* mice (β-cell alone) exhibited hyperglycemia, *MIP-PPG-MitoN* mice (both β-cell and α-cell) retained normoglycemia. Furthermore, although *MIP-MitoN* mice are glucose intolerant and lack insulin responses, *MIP-PPG-MitoN* mice hypersecrete insulin, indicating that dual induction of mitoNEET in both cell types (thus simultaneous cell impairment) is protective against mitoNEET-driven hyperglycemia and β-cell loss.

Given that both *PPG-MitoN* mice (α-cells) and *MIP-PPG-MitoN* mice (β- and α-cells) prevent the loss of β-cell mass typically seen in *MIP-MitoN* mice (β-cells), we transcriptionally screened for potential survival factors emanating from the perturbed α-cell that could protect the viability of the adjacent β-cell. Three genes profoundly upregulated in *PPG-MitoN* α-cells stood out as potential β-cytotrophic candidates: *Ngfa*, *Pdip*, and *Tff2* (Table 1). *Ngfa* is a critical neurotrophic factor that enhances GSIS to improve viability and survival of islets (52). Conversely, withdrawal or neutralization of *Ngfa* induces β-cell apoptosis (53) and lowers insulin levels (69). Future studies exploring the mechanisms of how a mitoNEET-mediated induction of *Ngfa* exerts autocrine antiapoptotic properties to maintain β-cell survival in a mouse model with dysregulated α-cell homeostasis (the *PPG-MitoN* mouse) should prove beneficial. Finally, further transcriptional screening of *PPG-MitoN* α-cells revealed a surprising switch in transcriptional patterning. Perturbed transgenic α-cells transcriptionally converted from an α-cell program to a more β-cell–like profile (Table 2). Although conversion of α-cells to β-cells has been reported after extreme β-cell loss (70), the complete rescue of β-cell mass in *PPG-MitoN* mice is unlikely to be exclusively due to a conversion of α-cells. This could be a result of more β-cells remaining than original α-cells present; additionally, there does not appear to be a net depletion of α-cells seemingly converting to β-cells.

In summary, we identify a novel inducible mitoNEET-driven mouse model of diabetes. Mechanistically, we show that mitoNEET enhances Parkin-mediated mitophagy, resulting in the formation of unique mitophagosomes in β-cells. We further characterize a novel α-cell–specific model of mitoNEET induction that causes a dysregulation in local glucagon homeostasis to unleash hypersecretion of insulin. Finally, we used mitoNEET to simultaneously disrupt α- and β-cell homeostasis, which exerts a protective effect by preserving β-cell viability. Figure 7*B* summarizes our three novel mouse models of β-cell and/or α-cell impairment, which highlight the importance of proper mitochondrial function in the maintenance of pancreatic function and, secondary to that, whole-body glucose homeostasis. We used these systems to define potent β-cytoprotective factors derived from α-cells with compromised mitochondrial function.

Acknowledgments. The authors thank J. Song and S. Connell (UTSW Medical Center, Dallas, TX) for technical assistance as well as the rest of the Scherer laboratory for helpful discussions. They also thank Pierre Cosson and Lelio Orci (Department of Cell Physiology and Metabolism, University of Geneva, Geneva, Switzerland) for valuable comments, Bob Hammer and the UTSW Transgenic Core Facility for the generation of mouse models, and the UTSW Metabolic Core Facility (Xioli Lin for perfusions for EM experiments) and EM Core Facility, particularly Rebecca Jackson, Robyn Leidel, Phoebe Doss, and Anza Darehshouri. Finally, the authors thank George Adams and Shengxi Liu (Nancy) at the Illumina Microarray Core of UTSW and Young Lee (UTSW Medical Center) for providing INS-1 cells.

Funding. C.M.K. was supported by a fellowship from JDRF International (3-2008-130). C.M.K. and P.E.Sc. were supported by a JDRF/Eli Lilly Company

Program Award (2-SRA-2016-149-Q-R; PI: William Holland). W.-h.L. was supported by National Institutes of Health grant R01-GM 077593. The authors were also supported by National Institutes of Health grants R01-DK-55758, R01-DK-099110, and P01-DK-088761 (to P.E.Sc.).

Duality of Interest. No potential conflicts of interest relevant to this article were reported.

Author Contributions. C.M.K. designed and performed all experiments, analyzed data, and contributed to the writing of the manuscript. S.C. and W.-h.L. performed the GSIS perfused pancreata experiments, isolated α-cells from *PPG-MitoN* mice for microarray analysis, and performed the $\Delta\Psi_m$ experiments. R.Y. contributed to the injections during the isolation of islets and performed the β-gal staining on *TRE-LacZ-MIP-rtTA* brain tissues. K.S. generated the *TRE-MitoN* mouse. Q.A.W. generated the *PPG-rtTA* mouse and contributed to the β-gal staining of *PPG-rtTA* tissues. S.B.S. generated the *MIP-rtTA* mouse. P.E.Sa. and J.T.B. contributed to the use of mass spectrometry to measure the various lipid species in islets isolated from the *MIP-MitoN* mice. W.J.G. was involved in key discussions that were critical to the mechanistic insights of the manuscript. R.H.U. provided expertise in islet biology. P.E.Sc. contributed to the experimental design, performance of experiments, data analysis and interpretation, and the writing of the manuscript. P.E.Sc. is the guarantor of this work and, as such, had full access to all the data in the study and takes responsibility for the integrity of the data and the accuracy of the data analysis.

References

1. Maechler P, Carobbio S, Rubi B. In beta-cells, mitochondria integrate and generate metabolic signals controlling insulin secretion. Int J Biochem Cell Biol 2006;38:696–709
2. Supale S, Li N, Brun T, Maechler P. Mitochondrial dysfunction in pancreatic β cells. Trends Endocrinol Metab 2012;23:477–487
3. Maechler P, de Andrade PB. Mitochondrial damages and the regulation of insulin secretion. Biochem Soc Trans 2006;34:824–827
4. Prentki M, Nolan CJ. Islet beta cell failure in type 2 diabetes. J Clin Invest 2006;116:1802–1812
5. Marchetti P, Lupi R, Del Guerra S, Bugliani M, Marselli L, Boggi U. The beta-cell in human type 2 diabetes. Adv Exp Med Biol 2010;654:501–514
6. Anello M, Lupi R, Spampinato D, et al. Functional and morphological alterations of mitochondria in pancreatic beta cells from type 2 diabetic patients. Diabetologia 2005;48:282–289
7. Muoio DM, Newgard CB. Obesity-related derangements in metabolic regulation. Annu Rev Biochem 2006;75:367–401
8. Lowell BB, Shulman GI. Mitochondrial dysfunction and type 2 diabetes. Science 2005;307:384–387
9. Silva JP, Köhler M, Graff C, et al. Impaired insulin secretion and beta-cell loss in tissue-specific knockout mice with mitochondrial diabetes. Nat Genet 2000;26:336–340
10. Colca JR, McDonald WG, Waldon DJ, et al. Identification of a novel mitochondrial protein ("mitoNEET") cross-linked specifically by a thiazolidinedione photoprobe. Am J Physiol Endocrinol Metab 2004;286:E252–E260
11. Paddock ML, Wiley SE, Axelrod HL, et al. MitoNEET is a uniquely folded 2Fe 2S outer mitochondrial membrane protein stabilized by pioglitazone. Proc Natl Acad Sci U S A 2007;104:14342–14347
12. Wiley SE, Paddock ML, Abresch EC, et al. The outer mitochondrial membrane protein mitoNEET contains a novel redox-active 2Fe-2S cluster. J Biol Chem 2007;282:23745–23749
13. Wiley SE, Murphy AN, Ross SA, van der Geer P, Dixon JE. MitoNEET is an iron-containing outer mitochondrial membrane protein that regulates oxidative capacity. Proc Natl Acad Sci U S A 2007;104:5318–5323
14. Lin J, Zhou T, Ye K, Wang J. Crystal structure of human mitoNEET reveals distinct groups of iron sulfur proteins. Proc Natl Acad Sci U S A 2007;104:14640–14645
15. Kusminski CM, Holland WL, Sun K, et al. MitoNEET-driven alterations in adipocyte mitochondrial activity reveal a crucial adaptive process that preserves insulin sensitivity in obesity. Nat Med 2012;18:1539–1549
16. Yamatani K, Saito K, Ikezawa Y, et al. Relative contribution of Ca2+-dependent mechanism in glucagon-induced glucose output from the liver. Arch Biochem Biophys 1998;355:175–180
17. Cherrington A, Vranic M. Role of glucagon and insulin in control of glucose turnover. Metabolism 1971;20:625–628
18. Dunning BE, Gerich JE. The role of alpha-cell dysregulation in fasting and postprandial hyperglycemia in type 2 diabetes and therapeutic implications. Endocr Rev 2007;28:253–283
19. Reaven GM, Chen YD, Golay A, Swislocki AL, Jaspan JB. Documentation of hyperglucagonemia throughout the day in nonobese and obese patients with noninsulin-dependent diabetes mellitus. J Clin Endocrinol Metab 1987;64:106–110
20. Unger RH, Cherrington AD. Glucagonocentric restructuring of diabetes: a pathophysiologic and therapeutic makeover. J Clin Invest 2012;122:4–12
21. Shah P, Vella A, Basu A, Basu R, Schwenk WF, Rizza RA. Lack of suppression of glucagon contributes to postprandial hyperglycemia in subjects with type 2 diabetes mellitus. J Clin Endocrinol Metab 2000;85:4053–4059
22. Mu J, Woods J, Zhou YP, et al. Chronic inhibition of dipeptidyl peptidase-4 with a sitagliptin analog preserves pancreatic beta-cell mass and function in a rodent model of type 2 diabetes. Diabetes 2006;55:1695–1704
23. Ye R, Holland WL, Gordillo R, et al. Adiponectin is essential for lipid homeostasis and survival under insulin deficiency and promotes β-cell regeneration. eLife 2014;3:3
24. Livak KJ, Schmittgen TD. Analysis of relative gene expression data using real-time quantitative PCR and the 2(-Delta Delta C(T)) Method. Methods 2001; 25:402–408
25. Li Z, Li Y, Chakraborty M, et al. Liver-specific deficiency of serine palmitoyltransferase subunit 2 decreases plasma sphingomyelin and increases apolipoprotein E levels. J Biol Chem 2009;284:27010–27019
26. Gannon M, Shiota C, Postic C, Wright CV, Magnuson M. Analysis of the Cre-mediated recombination driven by rat insulin promoter in embryonic and adult mouse pancreas. Genesis 2000;26:139–142
27. Mojsov S, Heinrich G, Wilson IB, Ravazzola M, Orci L, Habener JF. Preproglucagon gene expression in pancreas and intestine diversifies at the level of post-translational processing. J Biol Chem 1986;261:11880–11889
28. Blazquez E, Muñoz-Barragan L, Patton GS, Orci L, Dobbs RE, Unger RH. Gastric A-cell function in insulin-deprived depancreatized dogs. Endocrinology 1976;99:1182–1188
29. Henquin JC. Regulation of insulin secretion: a matter of phase control and amplitude modulation. Diabetologia 2009;52:739–751
30. Combs TP, Berg AH, Rajala MW, et al. Sexual differentiation, pregnancy, calorie restriction, and aging affect the adipocyte-specific secretory protein adiponectin. Diabetes 2003;52:268–276
31. Holland WL, Miller RA, Wang ZV, et al. Receptor-mediated activation of ceramidase activity initiates the pleiotropic actions of adiponectin. Nat Med 2011; 17:55–63
32. Lu H, Koshkin V, Allister EM, Gyulkhandanyan AV, Wheeler MB. Molecular and metabolic evidence for mitochondrial defects associated with beta-cell dysfunction in a mouse model of type 2 diabetes. Diabetes 2010; 59:448–459
33. Ichimura Y, Kirisako T, Takao T, et al. A ubiquitin-like system mediates protein lipidation. Nature 2000;408:488–492
34. Xie Z, Nair U, Klionsky DJ. Atg8 controls phagophore expansion during autophagosome formation. Mol Biol Cell 2008;19:3290–3298
35. Maechler P, Wollheim CB. Mitochondrial function in normal and diabetic beta-cells. Nature 2001;414:807–812
36. Martino L, Masini M, Novelli M, et al. Palmitate activates autophagy in INS-1E β-cells and in isolated rat and human pancreatic islets. PLoS One 2012;7: e36188
37. Aita VM, Liang XH, Murty VV, et al. Cloning and genomic organization of beclin 1, a candidate tumor suppressor gene on chromosome 17q21. Genomics 1999;59:59–65

38. Liang XH, Jackson S, Seaman M, et al. Induction of autophagy and inhibition of tumorigenesis by beclin 1. Nature 1999;402:672–676
39. Wang RC, Wei Y, An Z, et al. Akt-mediated regulation of autophagy and tumorigenesis through Beclin 1 phosphorylation. Science 2012;338:956–959
40. Sauvé V, Gehring K. Phosphorylated ubiquitin: a new shade of PINK1 in Parkin activation. Cell Res 2014;24:1025–1026
41. Trempe JF, Sauvé V, Grenier K, et al. Structure of Parkin reveals mechanisms for ubiquitin ligase activation. Science 2013;340:1451–1455
42. Jin HS, Kim J, Lee SJ, et al. The PARK2 gene is involved in the maintenance of pancreatic β-cell functions related to insulin production and secretion. Mol Cell Endocrinol 2014;382:178–189
43. Hoshino A, Ariyoshi M, Okawa Y, et al. Inhibition of p53 preserves Parkin-mediated mitophagy and pancreatic β-cell function in diabetes. Proc Natl Acad Sci U S A 2014;111:3116–3121
44. Lazarou M, Jin SM, Kane LA, Youle RJ. Role of PINK1 binding to the TOM complex and alternate intracellular membranes in recruitment and activation of the E3 ligase Parkin. Dev Cell 2012;22:320–333
45. Finney N, Walther F, Mantel PY, Stauffer D, Rovelli G, Dev KK. The cellular protein level of Parkin is regulated by its ubiquitin-like domain. J Biol Chem 2003; 278:16054–16058
46. Okatsu K, Kimura M, Oka T, Tanaka K, Matsuda N. Unconventional PINK1 localization to the outer membrane of depolarized mitochondria drives Parkin recruitment. J Cell Sci 2015;128:964–978
47. Lazarou M, Narendra DP, Jin SM, Tekle E, Banerjee S, Youle RJ. PINK1 drives Parkin self-association and HECT-like E3 activity upstream of mitochondrial binding. J Cell Biol 2013;200:163–172
48. Saltiel AR, Olefsky JM. Thiazolidinediones in the treatment of insulin resistance and type II diabetes. Diabetes 1996;45:1661–1669
49. Kawashima S, Matsuoka TA, Kaneto H, et al. Effect of alogliptin, pioglitazone and glargine on pancreatic β-cells in diabetic db/db mice. Biochem Biophys Res Commun 2011;404:534–540
50. Ishida H, Takizawa M, Ozawa S, et al. Pioglitazone improves insulin secretory capacity and prevents the loss of beta-cell mass in obese diabetic db/db mice: possible protection of beta cells from oxidative stress. Metabolism 2004;53:488–494
51. Wang ZV, Mu J, Schraw TD, et al. PANIC-ATTAC: a mouse model for inducible and reversible beta-cell ablation. Diabetes 2008;57:2137–2148
52. Miao G, Mace J, Kirby M, et al. In vitro and in vivo improvement of islet survival following treatment with nerve growth factor. Transplantation 2006;81:519–524
53. Pierucci D, Cicconi S, Bonini P, et al. NGF-withdrawal induces apoptosis in pancreatic beta cells in vitro. Diabetologia 2001;44:1281–1295
54. Orime K, Shirakawa J, Togashi Y, et al. Trefoil factor 2 promotes cell proliferation in pancreatic β-cells through CXCR-4-mediated ERK1/2 phosphorylation. Endocrinology 2013;154:54–64
55. Wiederkehr A, Wollheim CB. Mitochondrial signals drive insulin secretion in the pancreatic β-cell. Mol Cell Endocrinol 2012;353:128–137
56. Patti ME, Corvera S. The role of mitochondria in the pathogenesis of type 2 diabetes. Endocr Rev 2010;31:364–395
57. Jitrapakdee S, Wutthisathapornchai A, Wallace JC, MacDonald MJ. Regulation of insulin secretion: role of mitochondrial signalling. Diabetologia 2010;53: 1019–1032
58. Ohta M, Nelson D, Nelson J, Meglasson MD, Erecińska M. Oxygen and temperature dependence of stimulated insulin secretion in isolated rat islets of Langerhans. J Biol Chem 1990;265:17525–17532
59. Kennedy ED, Maechler P, Wollheim CB. Effects of depletion of mitochondrial DNA in metabolism secretion coupling in INS-1 cells. Diabetes 1998; 47:374–380
60. Lee MS. Role of islet β cell autophagy in the pathogenesis of diabetes. Trends Endocrinol Metab 2014;25:620–627
61. Geisler S, Holmström KM, Skujat D, et al. PINK1/Parkin-mediated mitophagy is dependent on VDAC1 and p62/SQSTM1. Nat Cell Biol 2010;12:119–131
62. Wongseree W, Assawamakin A, Piroonratana T, Sinsomros S, Limwongse C, Chaiyaratana N. Detecting purely epistatic multi-locus interactions by an omnibus permutation test on ensembles of two-locus analyses. BMC Bioinformatics 2009; 10:294
63. Leak TS, Mychaleckyj JC, Smith SG, et al. Evaluation of a SNP map of 6q24-27 confirms diabetic nephropathy loci and identifies novel associations in type 2 diabetes patients with nephropathy from an African-American population. Hum Genet 2008;124:63–71
64. Vives-Bauza C, Zhou C, Huang Y, et al. PINK1-dependent recruitment of Parkin to mitochondria in mitophagy. Proc Natl Acad Sci U S A 2010;107:378–383
65. Wild P, Dikic I. Mitochondria get a Parkin' ticket. Nat Cell Biol 2010;12:104–106
66. Unger RH, Orci L. Paracrinology of islets and the paracrinopathy of diabetes. Proc Natl Acad Sci U S A 2010;107:16009–16012
67. Hancock AS, Du A, Liu J, Miller M, May CL. Glucagon deficiency reduces hepatic glucose production and improves glucose tolerance in adult mice. Mol Endocrinol 2010;24:1605–1614
68. Lee Y, Wang MY, Du XQ, Charron MJ, Unger RH. Glucagon receptor knockout prevents insulin-deficient type 1 diabetes in mice. Diabetes 2011;60: 391–397
69. Gezginci-Oktayoglu S, Karatug A, Bolkent S. The relation among NGF, EGF and insulin is important for triggering pancreatic β cell apoptosis. Diabetes Metab Res Rev 2012;28:654–662
70. Thorel F, Népote V, Avril I, et al. Conversion of adult pancreatic alpha-cells to beta-cells after extreme beta-cell loss. Nature 2010;464:1149–1154